

Ground-state phase diagram and magnetic properties of a tetramerized spin- $\frac{1}{2}$ $J_1 - J_2$ model: BEC of bound magnons and absence of the transverse magnetization

H. T. Ueda and K. Totsuka

Yukawa Institute for Theoretical Physics, Kyoto University, Kitashirakawa Oiwake-Cho, Kyoto 606-8502, Japan

We study the ground state and the magnetization process of a spin- $1/2$ J_1 - J_2 model with a plaquette structure by using various methods. For small inter-plaquette interaction, this model is expected to have a spin-gap and we computed the first- and the second excitation energies. If the gap of the lowest excitation closes, the corresponding particle condenses to form magnetic orders. By analyzing the quintet gap and magnetic interactions among the quintet excitations, we find a spin-nematic phase around $J_1/J_2 \sim -2$ due to the strong frustration and the quantum effect. When high magnetic moment is applied, not the spin-1 excitations but the spin-2 ones soften and dictate the magnetization process. We apply a mean-field approximation to the effective Hamiltonian to find three different types of phases (a conventional BEC phase, “striped” supersolid phases and a $1/2$ -plateau). Unlike the BEC in spin-dimer systems, this BEC phase is not accompanied by transverse magnetization. Possible connection to the recently discovered spin-gap compound (CuCl)LaNb₂O₇ is discussed.

I. INTRODUCTION

Magnetic frustration have provided us with many intriguing topics e.g. the phenomena of order-by-disorder, the residual entropy at absolute zero temperature, disordered spin liquids, etc¹. There are a variety of models which are known to exhibit the so-called frustration effects. Among them, the $S = 1/2$ J_1 - J_2 model on a square lattice has been extensively investigated over the last two decades as one of the simplest models to study how frustration destroys magnetic orders and stabilizes paramagnetic phases. The model is defined by adding antiferromagnetic interactions on diagonal bonds to the ordinary Heisenberg antiferromagnet on a square lattice (see FIG. 1):

$$\mathcal{H} = J_1 \sum_{\text{n.n.}} \mathbf{S}_i \cdot \mathbf{S}_j + J_2 \sum_{\text{n.n.n.}} \mathbf{S}_i \cdot \mathbf{S}_j, \quad (1)$$

where the summations (n.n.) and (n.n.n.) are taken for the nearest-neighbor- and the second-neighbor (diagonal) pairs, respectively. In the classical ($S \nearrow \infty$) limit, the ground state is readily obtained by computing Fourier transform $J(\mathbf{k})$ of the exchange interactions and minimize it in the \mathbf{k} -space:

- $J_1 > 0, J_2 < J_1/2$: the ground state has Néel antiferromagnetic order (NAF).
- $J_2 > |J_1|/2$: the ground state consists of two interpenetrating Néel-ordered square lattices. First quantum correction fixes the relative angle between the two ordering directions and selects the so-called *collinear antiferromagnetic order* (CAF).
- otherwise: the ferromagnetic (FM) ground state is stabilized.

For $J_2 < 0$, the next-nearest-neighbor (diagonal) interaction gives rise to no frustration and only the case with $J_2 > 0$ is non-trivial. The case $J_1, J_2 > 0$ has been extensively studied in the context of spin-gap phases stabilized by the frustrating interactions. Chandra and Douçot² investigated the model in the large- S limit and concluded that a non-magnetic (neither NAF nor CAF) phase appeared around the classical phase boundary $J_2/J_1 = 1/2$. The most quantum case

$S = 1/2$ has been studied later both by numerical^{3,4} and by analytical methods^{5,6} (for other literatures, see, for instance, Refs. 7,8 and references cited therein). By now it is fairly well established that we have spin gapped phase(s) in the window $0.4 \lesssim J_2/J_1 \lesssim 0.6$ although the nature of the spin-gap phase(s) is still in controversy.

The case with $J_1 < 0, J_2 > 0$ has been less investigated and recent analyses^{9,10} suggested that there is another non-magnetic (probably spin-nematic) phase around the classical boundary $J_2/J_1 = -1/2$ between CAF and FM. From an experimental viewpoint, most compounds^{11,12} found so far correspond to the ordered phase (CAF) of the J_1 - J_2 model.

Recently, Kageyama *et al.* reported¹³ a new two-dimensional Cu-based compound (CuCl)LaNb₂O₇. In this compound, two-dimensional sheets consisting of Cu²⁺ and Cl⁻ are separated from each other by non-magnetic [LaNb₂O₇] layers and within each sheet the Cu²⁺ ions form a square lattice. The Cl⁻ ions are located at the center of plaquettes and from a naive Goodenough-Kanamori argument the $S = 1/2$ J_1 - J_2 model with $J_1 < 0$ and $J_2 > 0$ is suggested as the model Hamiltonian for (CuCl)LaNb₂O₇.

What is remarkable with this compound is that inelastic neutron scattering experiments¹³ observed a finite spin gap 2.3meV(=26.7K) above the spin-singlet ground state. Subsequently, high-field magnetization measurements¹⁴ were carried out to show that magnetization monotonically increased between two critical fields $H_{c1} = 10.3\text{T}$ and $H_{c2} = 30.1\text{T}$. The data for (i) the Weiss temperature and (ii) the saturation field H_{c2} in principle determine the coupling constants J_1 and J_2 . Unfortunately, none of the solutions (J_1, J_2) obtained in this way reproduced the spin-gap behavior¹⁴. Therefore, the usual J_1 - J_2 model does not seem to work.

The second intriguing point concerns the magnetization process. From the standard scenario¹⁵, the onset of magnetization at $H = H_{c1}$ in spin-gapped systems is understood as Bose-Einstein condensation (BEC, or superfluid onset, more precisely) of the lowest-lying triplet excitation (magnon) and the lower critical field H_{c1} at $T = 0$ is given by the spin gap Δ as $H_{c1} = \Delta/(g\mu_B)$. This BEC scenario has been confirmed in various spin gap compounds^{16,17,18}.

Recent specific-heat- and magnetization measurements¹⁹ for (CuCl)LaNb₂O₇ exhibited behavior typical of spin-BEC transitions and suggested that the magnetization-onset transition at H_{c1} may be described by BEC of a certain kind of magnetic excitations. However, we immediately find a serious difficulty when we try to understand this within the standard BEC scenario; the lower critical field $H_{c1} = 18.4\text{T}$ expected from the observed spin gap $\Delta = 2.3\text{meV}$ at the zero field (where the experimental value $g = 2.17$ is used) in the standard scenario is much larger than the observed value¹⁴ $H_{c1} = 10.3\text{T}$. One possible explanation for this discrepancy may be that a lower-lying triplet excitation which is responsible for the BEC was not observed in the neutron-scattering experiments because of selection rules. However, this seems unlikely since powder samples were used and usually one can hardly expect a perfect extinction of a certain triplet excitation in such powder samples. Neither susceptibility measurements¹³ nor NMR data²⁰ indicate such a hidden triplet excitation.

An alternative and a more appealing scenario would be that the BEC occurs not in a single-particle channel but in a multi-particle channel. That is, what condenses to support a spin-superfluid is a bound state of magnon excitations. The possibility of multi-magnon condensation has been proposed theoretically^{21,22} in the context of a *kinetic* quintet bound state in the Shastry-Sutherland model (see Ref.23 and references cited therein). In fact, gapped quintet excitations which come down as the external field is increased were observed in the ESR experiments²⁴ carried out for SrCu₂(BO₃)₂, whereas small Dzyaloshinskii-Moriya interactions hindered a quintet BEC from being observed in that compound (see also Ref.25).

One of the simplest J_1 - J_2 -like models which realize the above scenario and have a finite spin gap would be the $S = 1/2$ J_1 - J_2 model with a plaquette structure (see FIG. 1). A similar model ($J_1, J_2 > 0$) has been investigated to develop a plaquette series expansion⁵. In this paper, we mainly focus on the region $J_1 < 0, J_2 > 0$ where the quintet excitation is expected to play an important role in low-energy physics.

The organization of the present paper is as follows. In section II, we briefly recapitulate the problem of a single plaquette mainly to establish the notations. The coupling among plaquettes will be taken into account in section III by two different methods: (i) a plaquette extension of the bond-operator mean-field theory²⁶ and (ii) a perturbation expansion with respect to the inter-plaquette couplings. We find gapped triplets and quintet for small enough inter-plaquette couplings in both methods.

For larger values of inter-plaquette couplings, one of the gapped excitations softens and the form of the effective interactions among the soft excitations determines the resulting magnetic phases. By using the gaps obtained in the perturbation expansion, we determine the semi-quantitative phase diagram in section IV (see FIG. 10 and FIG. 12).

The effect of high magnetic field will be considered in section V. For high enough field compared with the spin gaps, we can approximate the low-energy sector by using only the singlet and the lowest excited state. For $J_1 < 0$, we may expect that the quintet touches the singlet ground state first

and a multi-particle BEC occurs. On general grounds, a single-particle (magnon) BEC phase is expected to have finite transverse magnetization. Actually, in the BEC phase of TlCuCl₃, the transverse magnetization has been observed in the experiment¹⁶. In the case of a multi-particle BEC, however, the transverse magnetization does not appear. To investigate the magnetization process, we shall keep only the singlet and the quintet to derive a hardcore boson model as the effective Hamiltonian valid in high enough magnetic field. A mean-field approximation³² will be applied to the resulting effective Hamiltonian to draw a full magnetization curve. Interesting phases (a 1/2-plateau and supersolids) will be discussed. According to the value of the parameters, we shall roughly classify the magnetization curve in FIG. 15.

A summary of the main results and the discussion on the connection to the spin-gap compound (CuCl)LaNb₂O₇ will be given in sections VI and VII, respectively. The equations omitted in the text will be summarized in the appendices.

II. PLAQUETTE STRUCTURE

We consider a spin-1/2 J_1 - J_2 model with a plaquette structure where the interactions among spin-1/2s are explicitly tetramerized (see FIG. 1). The model is made up of four-spin units (*plaquettes*) and the four sites constituting a single plaquette are connected by the nearest-neighbor- (J_1) and the second-neighbor- (J_2) interactions as is shown in FIG. 2). The inter-plaquette interactions (both the nearest-neighbor- and the diagonal) which connect those units are multiplied by a distortion constant λ ($0 \leq \lambda \leq 1$). This parameter may be thought of as modeling the distortion of the underlying lattice in a simple way. In the case of $\lambda = 1$, this model reduces to the homogeneous J_1 - J_2 model, while when $\lambda = 0$, the plaquettes are decoupled from each other.

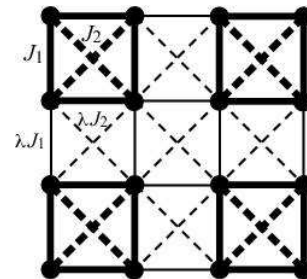


FIG. 1: Two dimensional square lattice with a plaquette structure to be considered in this paper. Filled circles denote spin-1/2s connected by the usual exchange interactions. Thin lines (both solid and broken) imply that the interactions are multiplied by the distortion parameter λ on these bonds.

A. single plaquette

Let us begin by analyzing a single isolated plaquette, which corresponds to the case $\lambda = 0$. The eigenstates of a single

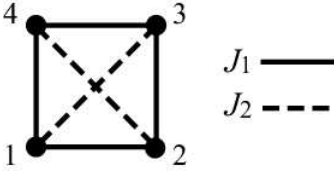


FIG. 2: Single plaquette. Dots represent spin 1/2s, and the solid- and the dashed lines respectively represent Heisenberg interaction with the couplings J_1 and J_2 between $S = 1/2$ spins.

plaquette can be easily obtained as follows. First we note that a plaquette Hamiltonian can be rewritten as

$$\begin{aligned} H &= J_1(\mathbf{S}_1 \cdot \mathbf{S}_2 + \mathbf{S}_2 \cdot \mathbf{S}_3 + \mathbf{S}_3 \cdot \mathbf{S}_4 + \mathbf{S}_4 \cdot \mathbf{S}_1) \\ &\quad + J_2(\mathbf{S}_1 \cdot \mathbf{S}_3 + \mathbf{S}_2 \cdot \mathbf{S}_4) \\ &= \frac{J_1}{2} \mathbf{S}^2 + \frac{1}{2}(J_2 - J_1)(\mathbf{S}_a^2 + \mathbf{S}_b^2) - \frac{3}{2}J_2, \end{aligned} \quad (2)$$

where $\mathbf{S}_a = \mathbf{S}_1 + \mathbf{S}_3$, $\mathbf{S}_b = \mathbf{S}_2 + \mathbf{S}_4$ and $\mathbf{S} = \mathbf{S}_a + \mathbf{S}_b$. Therefore, all the 2^4 eigenstates are classified by the three quantum numbers as $|S_a, S_b, S\rangle$. The eigenvalues $E(S_a, S_b, S)$ are given by

$$E(0, 0, 0) = 0, \quad (3a)$$

$$E(1, 1, 0) = 2J_2 - 2J_1, \quad (3b)$$

$$E(1, 0, 1) = E(0, 1, 1) = J_2, \quad (3c)$$

$$E(1, 1, 1) = -J_1 + 2J_2, \quad (3d)$$

$$E(1, 1, 2) = J_1 + 2J_2. \quad (3e)$$

Here a constant $-\frac{3}{2}J_2$ has been dropped just for simplicity. The energy of these states is shown in FIG. 3. For $-1 < J_1/J_2 < 0$, the spin-singlet state $|0, 0; 0\rangle$ is the ground state, the triplets $|1, 0; 1\rangle$, $|0, 1; 1\rangle$ are the first excited states, and the quintet $|1, 1; 2\rangle$ is the second excited state. For $-2 < J_1/J_2 < -1$, the singlet $|0, 0; 0\rangle$ is the ground state, quintet $|1, 1; 2\rangle$ is the first excited state, and triplets $|1, 0; 1\rangle$, $|0, 1; 1\rangle$ are the second excited state.

The singlet $|0, 0; 0\rangle$ is written as

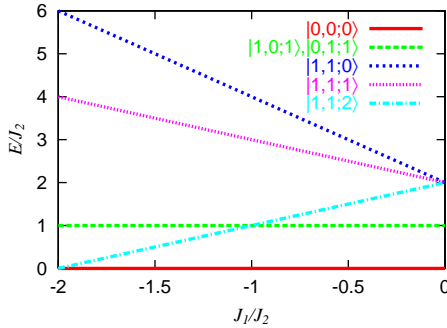


FIG. 3: The energy of the triplets $|1, 0; 1\rangle$, $|0, 1; 1\rangle$ and the quintet $|1, 1; 2\rangle$. We take the units of energy as J_2 , and the energy is plotted as a function of J_1/J_2

$$\begin{aligned} |s\rangle &\equiv |0, 0; 0\rangle \\ &= \frac{1}{2}(|\uparrow\downarrow\rangle - |\downarrow\uparrow\rangle)(|\uparrow\downarrow\rangle - |\downarrow\uparrow\rangle). \end{aligned} \quad (4)$$

In what follows, the single-spin states in ket will be shown in the order of 1,3,2,4, i.e. $|s_1, s_3, s_2, s_4\rangle$ in FIG. 2. For later convenience, we name the two triplets $|1, 0; 1\rangle$ and $|0, 1; 1\rangle$ as $|p_i\rangle$ and $|q_i\rangle$ ($i = x, y, z$) respectively. The explicit expressions of the two triplets are given as:

$$|p_x\rangle = -\frac{1}{2}(|\uparrow\uparrow\rangle - |\downarrow\downarrow\rangle)(|\uparrow\downarrow\rangle - |\downarrow\uparrow\rangle), \quad (5a)$$

$$|p_y\rangle = \frac{i}{2}(|\uparrow\uparrow\rangle + |\downarrow\downarrow\rangle)(|\uparrow\downarrow\rangle - |\downarrow\uparrow\rangle), \quad (5b)$$

$$|p_z\rangle = \frac{1}{2}(|\uparrow\downarrow\rangle + |\downarrow\uparrow\rangle)(|\uparrow\downarrow\rangle - |\downarrow\uparrow\rangle), \quad (5c)$$

$$|q_x\rangle = -\frac{1}{2}(|\uparrow\downarrow\rangle - |\downarrow\uparrow\rangle)(|\uparrow\uparrow\rangle - |\downarrow\downarrow\rangle), \quad (6a)$$

$$|q_y\rangle = \frac{i}{2}(|\uparrow\downarrow\rangle - |\downarrow\uparrow\rangle)(|\uparrow\uparrow\rangle + |\downarrow\downarrow\rangle), \quad (6b)$$

$$|q_z\rangle = \frac{1}{2}(|\uparrow\downarrow\rangle - |\downarrow\uparrow\rangle)(|\uparrow\downarrow\rangle + |\downarrow\uparrow\rangle). \quad (6c)$$

To label the quintet $|1, 1; 2\rangle$ states, we use the eigenvalues of S^z , i.e. $|1, 1; S=2, S^z\rangle$ whose expressions are given explicitly as:

$$|1, 1; 2, 2\rangle = |\uparrow\uparrow\uparrow\uparrow\rangle, \quad (7a)$$

$$|1, 1; 2, 1\rangle = \frac{1}{2}\{|\uparrow\uparrow\rangle(|\uparrow\downarrow\rangle + |\downarrow\uparrow\rangle) + (|\uparrow\downarrow\rangle + |\downarrow\uparrow\rangle)|\uparrow\uparrow\rangle\}, \quad (7b)$$

$$|1, 1; 2, 0\rangle = \frac{1}{\sqrt{6}}\{(|\uparrow\downarrow\rangle + |\downarrow\uparrow\rangle)(|\uparrow\downarrow\rangle + |\downarrow\uparrow\rangle) + |\uparrow\uparrow\downarrow\downarrow\rangle + |\downarrow\downarrow\uparrow\uparrow\rangle\}, \quad (7c)$$

$$|1, 1; 2, -1\rangle = \frac{1}{2}\{(|\downarrow\downarrow\rangle)(|\uparrow\downarrow\rangle + |\downarrow\uparrow\rangle) + (|\uparrow\downarrow\rangle + |\downarrow\uparrow\rangle)|\downarrow\downarrow\rangle\}, \quad (7d)$$

$$|1, 1; 2, -2\rangle = |\downarrow\downarrow\downarrow\downarrow\rangle. \quad (7e)$$

III. EFFECT OF INTER-PLAQUETTE INTERACTION

For $\lambda = 0$ and $J_1/J_2 > -2$, all plaquettes are in the singlet state $|0, 0; 0\rangle$. Finite inter-plaquette interactions λ induce various tunneling processes among plaquettes to change both the ground state and the excitations over it. For finite λ , we calculate the excitation energy by two different approaches. One is the bond-operator mean-field theory (MFT)^{26,33}, which gives the excitation energy of the triplets $|p_i\rangle$, $|q_i\rangle$. Another is the second-order perturbation theory in λ , and it gives the energy of the quintet $|1, 1; 2\rangle$ as well as that of $|p_i\rangle$ and $|q_i\rangle$. For sufficiently small λ , both approximations yield finite energy gaps for these excitations and when one of these gaps closes, the corresponding (bosonic) excitation condenses to form a

magnetically ordered state. The energy of triplet excitations can be observed by inelastic neutron scattering experiments. Both approximations may not be reliable for large λ and small $|J_1/J_2|$.

A. bond-operator MFT

Let us begin with the bond-operator MFT^{26,33}. For $-2 < J_1/J_2 < 0$ and $\lambda = 0$, $|0, 0; 0\rangle$ is the ground state and the degenerate triplets $|1, 0; 1\rangle$, $|0, 1; 1\rangle$ are the first- or the second excited state (see FIG. 3). Therefore, we may truncate the Hilbert space and consider a subspace spanned by the singlet $|0, 0; 0\rangle$ and the triplets $|p_i\rangle$, $|q_i\rangle$. This approximation is reliable to estimate the excitation energy of the triplets, unless $|1, 1; 2\rangle$ condenses. In this subspace, nonzero matrix elements of $\mathbf{S}_{1,2,3,4}$ is

$$\langle s | S_1^\alpha | p_\beta \rangle = \frac{1}{2} \delta_{\alpha\beta}, \quad \langle p_\alpha | S_1^\beta | p_\gamma \rangle = \frac{i}{2} \epsilon_{\alpha\beta\gamma}, \quad (8a)$$

$$\langle s | S_2^\alpha | q_\beta \rangle = \frac{1}{2} \delta_{\alpha\beta}, \quad \langle q_\alpha | S_2^\beta | q_\gamma \rangle = \frac{i}{2} \epsilon_{\alpha\beta\gamma}, \quad (8b)$$

$$\langle s | S_3^\alpha | p_\beta \rangle = -\frac{1}{2} \delta_{\alpha\beta}, \quad \langle p_\alpha | S_3^\beta | p_\gamma \rangle = \frac{i}{2} \epsilon_{\alpha\beta\gamma}, \quad (8c)$$

$$\langle s | S_4^\alpha | q_\beta \rangle = -\frac{1}{2} \delta_{\alpha\beta}, \quad \langle q_\alpha | S_4^\beta | q_\gamma \rangle = \frac{i}{2} \epsilon_{\alpha\beta\gamma}, \quad (8d)$$

where $\alpha, \beta = x, y, z$. Using boson operators s, p_α, q_α ($\alpha = x, y, z$) satisfying the standard commutation relations, $[s, s^\dagger] = 1$, $[p_\alpha, p_\beta^\dagger] = \delta_{\alpha\beta}$, $[q_\alpha, q_\beta^\dagger] = \delta_{\alpha\beta}$, $[s, p_\alpha] = 0$, etc, the local spin operator $\mathbf{S}_{1,2,3,4}$ can be written as

$$S_1^\alpha = \frac{1}{2} (s^\dagger p_\alpha + s p_\alpha^\dagger) - \frac{i}{2} \epsilon_{\alpha\beta\gamma} p_\beta^\dagger p_\gamma, \quad (9a)$$

$$S_3^\alpha = -\frac{1}{2} (s^\dagger p_\alpha + s p_\alpha^\dagger) - \frac{i}{2} \epsilon_{\alpha\beta\gamma} p_\beta^\dagger p_\gamma, \quad (9b)$$

$$S_2^\alpha = \frac{1}{2} (s^\dagger q_\alpha + s q_\alpha^\dagger) - \frac{i}{2} \epsilon_{\alpha\beta\gamma} q_\beta^\dagger q_\gamma, \quad (9c)$$

$$S_4^\alpha = -\frac{1}{2} (s^\dagger q_\alpha + s q_\alpha^\dagger) - \frac{i}{2} \epsilon_{\alpha\beta\gamma} q_\beta^\dagger q_\gamma, \quad (9d)$$

where the summation over repeated indices is implied. Since the restriction that each plaquette has exactly one particle leads to the local constraint $s^\dagger s + \sum_\alpha (p_\alpha^\dagger p_\alpha + q_\alpha^\dagger q_\alpha) = 1$, we introduce the Lagrange multiplier μ_i and add a term

$$\mu_i \left\{ s_i^\dagger s_i + \sum_\alpha (p_{\alpha,i}^\dagger p_{\alpha,i} + q_{\alpha,i}^\dagger q_{\alpha,i}) - 1 \right\}. \quad (10)$$

to each plaquette Hamiltonian. We may assume that μ_i for each plaquette takes the same value μ for all plaquettes because of the translation invariance.

Next, we replace s by its expectation value $\langle s \rangle = \bar{s}$, since the s boson condenses in the ground state. Moreover, since the triplet is dilute when the energy gap is positive, we may ignore the terms consisting of three or four triplet operators. In this way, we obtain the mean-field Hamiltonian H_{bo} consists only of bilinear terms in p and q . The mean-field parameters (μ, \bar{s}) are determined by requiring the expectation values

of the derivatives of H_{bo} with respect to the mean-field (MF) ground state vanish:

$$\left\langle \frac{\partial H_{\text{bo}}}{\partial \mu} \right\rangle_{\text{MF}} = 0, \quad \left\langle \frac{\partial H_{\text{bo}}}{\partial \bar{s}} \right\rangle_{\text{MF}} = 0, \quad (11)$$

or equivalently by finding the extrema of the mean-field ground-state energy $E_{\text{G.S.}}^{\text{mf}}$:

$$\frac{\partial E_{\text{G.S.}}^{\text{mf}}}{\partial \mu} = 0, \quad \frac{\partial E_{\text{G.S.}}^{\text{mf}}}{\partial \bar{s}} = 0. \quad (12)$$

In particular, $E_{\text{G.S.}}^{\text{mf}}$ must be minimum for \bar{s} .

In this approximation, the inter-plaquette interactions associated with the site n reads

$$\begin{aligned} (H_{\hat{x}})_n &= J_1 (\mathbf{S}_2 \cdot \mathbf{S}_a + \mathbf{S}_3 \cdot \mathbf{S}_b) + J_2 (\mathbf{S}_3 \cdot \mathbf{S}_a + \mathbf{S}_2 \cdot \mathbf{S}_b) \\ &= \frac{J_1}{4} \bar{s}^2 \{ (q_\alpha + q_\alpha^\dagger)_n (p_\alpha + p_\alpha^\dagger)_{n+\hat{x}} + (p_\alpha + p_\alpha^\dagger)_n (q_\alpha + q_\alpha^\dagger)_{n+\hat{x}} \} \\ &\quad - \frac{J_2}{4} \bar{s}^2 \{ (p_\alpha + p_\alpha^\dagger)_n (p_\alpha + p_\alpha^\dagger)_{n+\hat{x}} + (q_\alpha + q_\alpha^\dagger)_n (q_\alpha + q_\alpha^\dagger)_{n+\hat{x}} \}, \end{aligned} \quad (13a)$$

$$\begin{aligned} (H_{\hat{y}})_n &= J_1 (\mathbf{S}_3 \cdot \mathbf{S}_d + \mathbf{S}_4 \cdot \mathbf{S}_c) + J_2 (\mathbf{S}_3 \cdot \mathbf{S}_c + \mathbf{S}_4 \cdot \mathbf{S}_d) \\ &= -\frac{J_1}{4} \bar{s}^2 \{ (q_\alpha + q_\alpha^\dagger)_n (p_\alpha + p_\alpha^\dagger)_{n+\hat{y}} + (p_\alpha + p_\alpha^\dagger)_n (q_\alpha + q_\alpha^\dagger)_{n+\hat{y}} \} \\ &\quad - \frac{J_2}{4} \bar{s}^2 \{ (p_\alpha + p_\alpha^\dagger)_n (p_\alpha + p_\alpha^\dagger)_{n+\hat{y}} + (q_\alpha + q_\alpha^\dagger)_n (q_\alpha + q_\alpha^\dagger)_{n+\hat{y}} \}, \end{aligned} \quad (13b)$$

$$\begin{aligned} (H_{\hat{x}+\hat{y}})_n &= J_2 \mathbf{S}_3 \cdot \mathbf{S}_g \\ &= -\frac{J_2}{4} \bar{s}^2 (p_\alpha + p_\alpha^\dagger)_n (p_\alpha + p_\alpha^\dagger)_{n+\hat{x}+\hat{y}}, \end{aligned} \quad (13c)$$

$$\begin{aligned} (H_{\hat{x}-\hat{y}})_n &= J_2 \mathbf{S}_2 \cdot \mathbf{S}_f \\ &= -\frac{J_2}{4} \bar{s}^2 (q_\alpha + q_\alpha^\dagger)_n (q_\alpha + q_\alpha^\dagger)_{n+\hat{x}-\hat{y}}, \end{aligned} \quad (13d)$$

where the site labels $1, \dots, 4$ and a, \dots, g are defined in FIG. 4.

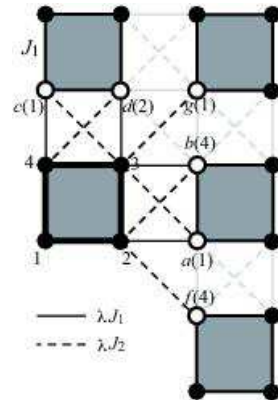


FIG. 4: Inter-plaquette interactions associated with the plaquette n (shown by a thick line).

Summing up all four interactions and doing Fourier trans-

formation, the total Hamiltonian H_{bo} reads

$$\begin{aligned}
H_{\text{bo}} = \sum_{\mathbf{k}} \left\{ & J_2 (p_{\mathbf{k}}^{\dagger\alpha} p_{\mathbf{k}}^{\alpha} + q_{\mathbf{k}}^{\dagger\alpha} q_{\mathbf{k}}^{\alpha}) \right. \\
& - \frac{J_2 \bar{s}^2}{4} f_+(\mathbf{k}) (p_{\mathbf{k}}^{\dagger\alpha} p_{\mathbf{k}}^{\alpha} + p_{\mathbf{k}}^{\alpha} p_{\mathbf{k}}^{\dagger\alpha} + p_{\mathbf{k}}^{\alpha} p_{-\mathbf{k}}^{\alpha} + p_{\mathbf{k}}^{\dagger\alpha} p_{-\mathbf{k}}^{\dagger\alpha}) \\
& - \frac{J_2 \bar{s}^2}{4} f_-(\mathbf{k}) (q_{\mathbf{k}}^{\dagger\alpha} q_{\mathbf{k}}^{\alpha} + q_{\mathbf{k}}^{\alpha} q_{\mathbf{k}}^{\dagger\alpha} + q_{\mathbf{k}}^{\alpha} q_{-\mathbf{k}}^{\alpha} + q_{\mathbf{k}}^{\dagger\alpha} q_{-\mathbf{k}}^{\dagger\alpha}) \\
& + \frac{J_1 \bar{s}^2}{2} (\cos k_x - \cos k_y) (p_{\mathbf{k}}^{\dagger\alpha} q_{\mathbf{k}}^{\alpha} + p_{\mathbf{k}}^{\alpha} q_{-\mathbf{k}}^{\alpha} + h.c.) \\
& \left. - \mu (\bar{s}^2 + p_{\mathbf{k}}^{\dagger\alpha} p_{\mathbf{k}}^{\alpha} + q_{\mathbf{k}}^{\dagger\alpha} q_{\mathbf{k}}^{\alpha} - 1) \right\}, \quad (14a)
\end{aligned}$$

where we have defined

$$f_{\pm}(\mathbf{k}) \equiv \cos k_x + \cos k_y + \cos(k_x \pm k_y). \quad (15)$$

If we introduce a vector $\mathbf{v}_{\mathbf{k}} = (p_{\mathbf{k}}, q_{\mathbf{k}}, p_{-\mathbf{k}}^{\dagger}, q_{-\mathbf{k}}^{\dagger})^T$, the MF Hamiltonian H_{bo} can be written compactly as

$$H_{\text{bo}} = \sum_{\mathbf{k}} \mathbf{v}_{\mathbf{k}}^{\dagger\alpha} A(\mathbf{k}) \mathbf{v}_{\mathbf{k}}^{\alpha} - N_p \{3(J_2 - \mu) + \mu(\bar{s}^2 - 1)\}, \quad (16)$$

where N_p denotes the total number of plaquettes and the kernel $A(\mathbf{k})$ is given as

$$A(\mathbf{k}) = \begin{pmatrix} a_{\text{bo}}(\mathbf{k}) & b_{\text{bo}}(\mathbf{k}) & c_{\text{bo}}(\mathbf{k}) & d_{\text{bo}}(\mathbf{k}) \\ b_{\text{bo}}(\mathbf{k}) & e_{\text{bo}}(\mathbf{k}) & b_{\text{bo}}(\mathbf{k}) & d_{\text{bo}}(\mathbf{k}) \\ c_{\text{bo}}(\mathbf{k}) & b_{\text{bo}}(\mathbf{k}) & a_{\text{bo}}(\mathbf{k}) & b_{\text{bo}}(\mathbf{k}) \\ b_{\text{bo}}(\mathbf{k}) & d_{\text{bo}}(\mathbf{k}) & b_{\text{bo}}(\mathbf{k}) & e_{\text{bo}}(\mathbf{k}) \end{pmatrix}, \quad (17a)$$

$$a_{\text{bo}}(\mathbf{k}) = \frac{J_2}{2} - \frac{J_2 \bar{s}^2}{4} f_+(\mathbf{k}) - \frac{\mu}{2}, \quad (18a)$$

$$b_{\text{bo}}(\mathbf{k}) = -\frac{J_1 \bar{s}^2}{4} (\cos k_x - \cos k_y), \quad (18b)$$

$$c_{\text{bo}}(\mathbf{k}) = -\frac{J_2}{4} f_+(\mathbf{k}), \quad (18c)$$

$$d_{\text{bo}}(\mathbf{k}) = -\frac{J_2}{4} f_-(\mathbf{k}), \quad (18d)$$

$$e_{\text{bo}}(\mathbf{k}) = \frac{J_2}{2} - \frac{J_2 \bar{s}^2}{4} f_-(\mathbf{k}) - \frac{\mu}{2}. \quad (18e)$$

Using a 4×4 real matrix $L_{\mathbf{k}}$ (see Appendix A for the detail), we can diagonalize $A(\mathbf{k})$ by the Bogoliubov transformation:

$$\begin{aligned}
L_{\mathbf{k}} \mathbf{v}_{\mathbf{k}} &= \mathbf{v}'_{\mathbf{k}}, \\
\mathbf{v}'_{\mathbf{k}} &= \left(p'_{\mathbf{k}}, q'_{\mathbf{k}}, p'_{-\mathbf{k}}, q'_{-\mathbf{k}} \right)^T. \quad (19)
\end{aligned}$$

As is shown in Appendix A, H_{bo} then reduces to

$$H_{\text{bo}} = \sum_{\mathbf{k}} \left\{ \omega_1(\mathbf{k}) p_{\mathbf{k}}^{\dagger\alpha} p_{\mathbf{k}}^{\alpha} + \omega_2(\mathbf{k}) q_{\mathbf{k}}^{\dagger\alpha} q_{\mathbf{k}}^{\alpha} \right\} + E_{\text{G.S.}}^{\text{mf}}, \quad (20)$$

where the mean-field ground state energy is given as:

$$E_{\text{G.S.}}^{\text{mf}} = \sum_{\mathbf{k}} \left\{ \frac{3}{2} (\omega_1(\mathbf{k}) + \omega_2(\mathbf{k})) - 3(J_2 - \mu) - \mu(\bar{s}^2 - 1) \right\}, \quad (21a)$$

$$(\omega_1(\mathbf{k}), \omega_2(\mathbf{k})) = (\omega_{(+,-)}(\mathbf{k}), \omega_{(+,+)}(\mathbf{k})), \quad (21b)$$

$$\begin{aligned}
\omega_{(\pm,\pm)} &= \pm \frac{1}{2} \left[a^2 - c^2 - d^2 + e^2 \pm \{ (-a^2 + c^2 + d^2 - e^2)^2 \right. \\
&\quad \left. + 4(a-d)(c-e)(-4b^2 + ac + cd + ae + de) \}^{\frac{1}{2}} \right]^{\frac{1}{2}}. \quad (21c)
\end{aligned}$$

In eq. (21c), the order of signs \pm coincides on both sides. Since $\omega_{1,2} \geq 0$, condensation of the triplets p and q occurs when the equality holds at some \mathbf{k} . Otherwise, there is no condensation, and $\langle p_{\mathbf{k}}^{\alpha} \rangle = \langle q_{\mathbf{k}}^{\alpha} \rangle = 0$. Therefore, there exist rotational symmetry and no magnetic order. In this case, $\omega_{1,2}$ are the excitation energy of triplets.

We looked for the solutions (μ, \bar{s}) to the set of equations (12) numerically. For example, we found $(\mu, \bar{s}) = (-0.09, 0.96)$ for the set of parameters $\lambda = 0.3$, $J_1/J_2 = -0.8$. The dispersion relation of the excitation energy $\omega_1(\mathbf{k}) = \omega_{(+,-)}(\mathbf{k})$ is shown in FIG. 5.

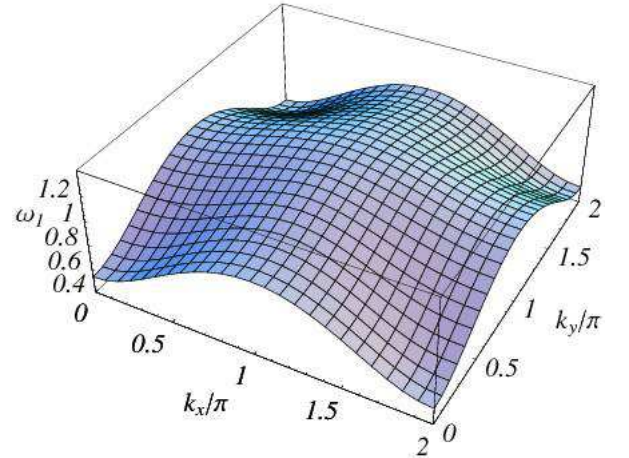


FIG. 5: The dispersion relation of the excitation energy of the triplet p' in (20), which has the lower energy of the two triplets, for the parameters $\lambda = 0.3$, $J_1 = -0.8$, $J_2 = 1$

If the excitation becomes soft $\omega = 0$ at some \mathbf{k} , the system is in a magnetically ordered phase. From the known results^{9,10}, we expect that ordered phase appears for λ sufficiently close to 1. To determine the phase boundary between the paramagnetic phase and magnetically ordered ones, we searched the $(\lambda, J_1/J_2)$ plane for the points where the mean-field gap vanishes. Unfortunately we found that the gap did not close in the relevant parameter region $0 < \lambda < 1$, $-2 < J_1/J_2 < 0$, and that the disordered singlet phase persisted; the gap vanished only for larger $\lambda (> 1)$. This unacceptable result may be attributed to the fact that the bond-operator mean-field theory probably overestimates the stability of the plaquette phase.

B. Second order perturbation

In this section, we compute the energy gap of triplets $|1, 0; 1\rangle$, $|0, 1; 1\rangle$ and the quintet $|1, 1; 2\rangle$ by the second order perturbation theory in the distortion parameter λ . The naive expansion in λ is ill-behaved in the vicinity of the point $J_1/J_2 = -2$ and we have to use another perturbation scheme for that region.

1. The excitation energies of triplets

Let us consider the states where there exists only one triplet and all the other plaquettes are in the singlet $|0, 0; 0\rangle$ state. If the coupling constant of inter-plaquette interaction $\lambda=0$, these states are N_p -fold degenerate, where N_p is the number of plaquettes. For finite λ , the second order perturbation induces hopping of the triplet to nearest or next nearest neighbors and lifts the degeneracy.

Rotational symmetry forbids the hopping which changes the spin label $i(= x, y, z)$ or the magnetic quantum number. On the other hands, the transitions between two different triplets p_i and q_i of the same label i occur. For example, the hopping amplitude of $p_i(q_i)$ to the nearest-neighbor plaquette is given by

$$-\frac{\lambda}{4}J_2 - \frac{\lambda^2}{8}J_2 \quad (22)$$

The degeneracy is partially resolved by the hopping of $p_i(q_i)$. The transition between p_i and q_i will be considered later. In the second-order perturbation, the processes that the triplet returns to the original site is also allowed. Including this effect, the energy change of $p_i(\mathbf{k})$ -particle is given by $a(\mathbf{k})$ in (D1). Similarly, that of $q_i(\mathbf{k})$ is given by $b(\mathbf{k})$ in (D2).

Next, we consider the transition between $p_i(\mathbf{k})$ and $q_i(\mathbf{k})$. The transition amplitude is given by

$$c(\mathbf{k}) \equiv \left(\frac{J_1}{2}\lambda + \frac{J_1^2}{4J_2}\lambda^2 \right) (\cos k_x - \cos k_y). \quad (23)$$

Therefore, for each $i = (x, y, z)$, eigenstates t_+ , t_- satisfies

$$\begin{pmatrix} a(\mathbf{k}) & c(\mathbf{k}) \\ c(\mathbf{k}) & b(\mathbf{k}) \end{pmatrix} \begin{pmatrix} t_{\pm}^{(1)} \\ t_{\pm}^{(2)} \end{pmatrix} = E(\mathbf{k}) \begin{pmatrix} t_{\pm}^{(1)} \\ t_{\pm}^{(2)} \end{pmatrix} \quad (24)$$

The expressions of $a(\mathbf{k})$, $b(\mathbf{k})$, $c(\mathbf{k})$ are given in Appendix D. After this procedure, the degeneracy with respect both to the position and to the species p_i and q_i is resolved. There also exists an energy shift in the ground state. Taking all these into account, we obtain the energy of the triplets:

$$E_t^{\pm}(\mathbf{k}) = \frac{1}{2} \left(a(\mathbf{k}) + b(\mathbf{k}) \pm \sqrt{(a(\mathbf{k}) - b(\mathbf{k}))^2 + 4c(\mathbf{k})^2} \right) - \Delta E_s, \quad (25)$$

where ΔE_s denotes the energy shift of the bare ground state where all plaquettes are occupied by the singlet $|0, 0; 0\rangle$ and is

given by eq.(D4). The dispersion relation of the lower branch E_t^- is shown in FIG. 6

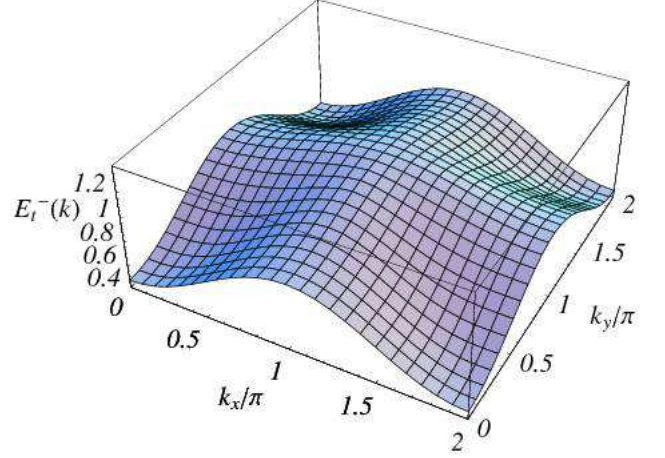


FIG. 6: The dispersion relation of the excitation energy $E_t^-(\mathbf{k})$ of triplet at $\lambda = 0.3$, $J_1 = -0.8$, $J_2 = 1$.

The lower branch E_t^- takes its minimum at the Γ -point $\mathbf{k} = 0$, and $E_t^-(\mathbf{k} = 0)$ gives spin gap Δ_t . The second order expression of Δ_t is given in (D5). The expression tells us that Δ_t has a pole at $J_1 = -2J_2$ and that the standard perturbation breaks down near the pole. To remedy this, we introduce another perturbation parameter $\delta = J_1 - (-2J_2)$ and carry out a double expansion in both λ and δ . Then, we obtain the energy gap in a modified method $E_{t,\text{mod}}^-(0)$ given in eq.(D6). This improved energy gap is expressed to give a better approximation around $J_1 = -2J_2$

2. excitation energy of quintet

Next, we consider states containing only one quintet in a background of the singlet plaquettes. As before, the degeneracy with respect to the position of the quintet plaquette is resolved by hopping. Up to the second order in λ , the hopping to nearest neighbor is given by

$$\lambda^2 \frac{J_1^2 + J_2^2}{8J_1} \quad (26)$$

and the hopping to next nearest neighbor does not occur. Taking into account the processes that the quintet returns to the original site and the energy shift of the ground state, the excitation energy of quintet is given by $E_q(\mathbf{k})$ in (D7). The dispersion relation is shown in FIG. 7

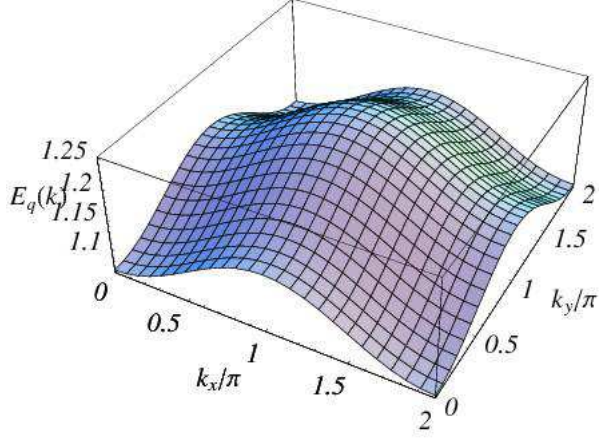


FIG. 7: The dispersion relation of the excitation energy $E_q(\mathbf{k})$ of quintet at $\lambda = 0.3$, $J_1 = -0.8$, $J_2 = 1$.

Since the quintet dispersion $E_q(\mathbf{k})$ takes its minimum at $\mathbf{k} = \mathbf{0}$, the quintet gap is given by

$$\begin{aligned} \Delta_q &\equiv E_q(\mathbf{k} = \mathbf{0}) \\ &= J_1 + 2J_2 - \frac{\lambda^2(6J_1^3 - 23J_1J_2 + 10J_2^3)}{8J_1(2J_1 - J_2)}. \end{aligned} \quad (27)$$

We note that there is the pole at $J_1 = 0$ and the approximation becomes poor for $J_1 \approx 0$.

IV. GROUND STATE PHASES

If the inter-plaquette coupling λ is increased, one of the energy gaps of the triplets ((D5) and (D6)) and the quintet (D7) becomes 0 at a certain critical value of λ . When it happens, the corresponding particle condenses and a phase transition occurs from the gapped spin-singlet phase to superfluid phases with magnetic long-range order. Therefore, we can classify the phases according to what kind of particles condense and what kind of magnetic orders is stabilized by a given set of interactions among them. In FIGs. 8 and 9, we plot the value of λ at which the smallest energy gap becomes 0. If we assume that no further condensation occurs in the other kinds of particles once the triplets or the quintet condenses, the phase diagram FIG. 10 is obtained. When we mapped out the phase diagram FIG. 10, we have used two different expressions (D6) and (D5) for the energy gap of the lowest triplet in the vicinity of $J_1/J_2 = -2$ and away from it ($J_1/J_2 \sim 0$), respectively. We have also neglected the quintet around $J_1/J_2 = 0$ since the collapse of the quintet gap there (see FIG. 8) can be attributed to the existence of a pole and is just an artifact of the perturbative approximation. Note that the phase boundary between the two regions covered by eq.(D5) and eq.(D6) is only schematic.

Now let us discuss the nature of the ordered phases appearing after the condensation. In the region shown as ‘‘CAF’’

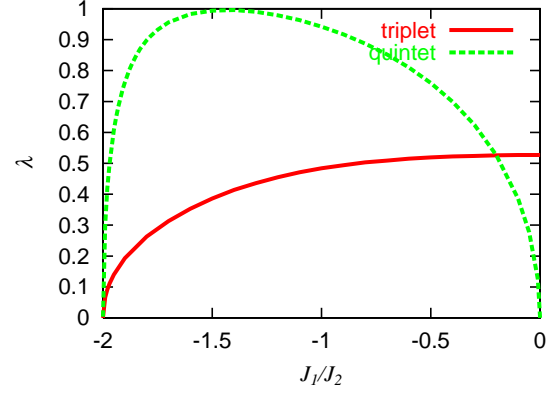


FIG. 8: The value of λ at which the energy gaps Δ_t and Δ_q close. The energy gap of the triplets Δ_t is given in (D5), which is not reliable near $J_1/J_2 = -2$ because of the pole there, and that of the quintet Δ_q is in (27), which is not reliable near $J_1/J_2 = 0$.

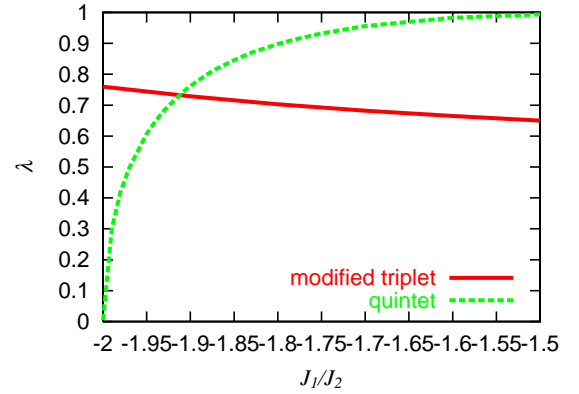


FIG. 9: Plot of the value of λ when the energy gaps are equal to 0. We use $\Delta_{t,\text{mod}}$ (eq.(D6)) for the triplets, which is reliable even in the vicinity of $J_1/J_2 = -2$. The curve for the quintet is the same as in FIG. 8. We only plot the region $-2 < J_1/J_2 < -1.5$.

(highlighted in red) in FIG. 10, condensation occurs to the singlet and the triplets. Then, we may expect:

$$|\langle s \rangle| \neq 0, |\langle \mathbf{p}(\mathbf{k} = \mathbf{0}) \rangle|^2 \neq 0, |\langle \mathbf{q}(\mathbf{k} = \mathbf{0}) \rangle|^2 \neq 0, \quad (28)$$

which, combined with (9d), implies

$$\langle \mathbf{S}_1 \rangle = -\langle \mathbf{S}_3 \rangle \neq 0, \quad (29a)$$

$$\langle \mathbf{S}_2 \rangle = -\langle \mathbf{S}_4 \rangle \neq 0, \quad (29b)$$

provided that $\epsilon^{\alpha\beta\gamma} \langle p_\beta^\dagger \rangle \langle p_\gamma \rangle = 0$ and $\epsilon^{\alpha\beta\gamma} \langle q_\beta^\dagger \rangle \langle q_\gamma \rangle = 0$. Note that all the plaquettes are in the same state, since the energy of the triplet takes its minimum at the Γ -point $\mathbf{k} = \mathbf{0}$ (see FIG. 6). When the combination $(\mathbf{p} + \mathbf{q})$ of the two bosons condenses, the relation $\langle \mathbf{S}_1 \rangle = \langle \mathbf{S}_2 \rangle$ holds and the ground state has the transversely aligned (i.e. $(0, \pi)$) collinear antiferromagnetic order. In the case where $(\mathbf{p} - \mathbf{q})$ condenses, on the other hand, we have $\langle \mathbf{S}_1 \rangle = -\langle \mathbf{S}_2 \rangle$ instead and the system

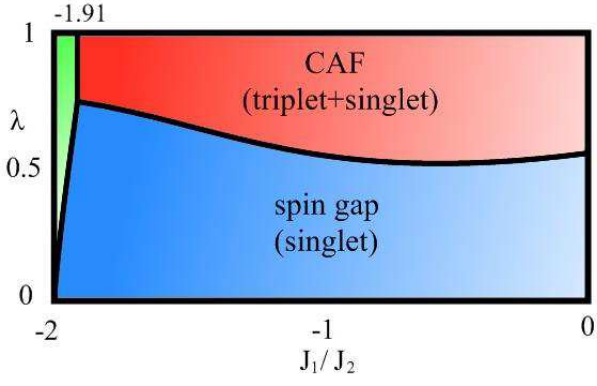


FIG. 10: The schematic phase diagram of the ground state determined by the particle whose excitation gap closes first. In the green region, the quintet and the singlet condense, in the red do the triplet and the singlet, and in the blue does the singlet. In the region marked by blue, the energy gap exists. The phase shown by red may be considered as collinear antiferromagnetic (CAF) state. The nature of the green phase, where the quintet condensation occurs, is closely investigated by using an effective Hamiltonian H_{qu} (eq.(32)).

is in the collinear antiferromagnetic ground state in the longitudinal $((\pi, 0))$ direction. This is consistent with the known results⁹.

Now we move on to a more interesting case. In the green region in FIG. 10, frustration is strong ($J_2 \approx -2J_1$) and non-trivial order may be expected. In fact, Shannon *et al.*^{9,10} analyzed the uniform ($\lambda = 1$) model by numerical exact diagonalizations up to clusters of 36 spins and found a spin-nematic phase with d -wave (or B_1) symmetry for $-2.5 < J_1/J_2 < -1.43 \sim -1.67$. In the state with the nematic order, the expectation value of the rank-1 tensor vanishes $\langle \mathbf{S}_i \rangle = 0$, while we have a finite expectation value of the following traceless rank-2 tensor:

$$Q_{ij}^{\alpha\beta} \equiv \frac{S_i^\alpha S_j^\beta + S_i^\beta S_j^\alpha}{2} - \frac{\mathbf{S}_i \cdot \mathbf{S}_j}{3} \delta^{\alpha\beta}, \quad (30)$$

where $\alpha, \beta = (x, y, z)$ and i, j label the lattice sites.

As is shown in FIG. 10, the singlet and the quintet condense in the region of interest. This is analogous to the spinor Bose-Einstein condensation of spin-2 particles (here particles are defined not on the lattice sites but on the plaquettes). We consider a single plaquette (see FIG. 2) and, as before, denote the singlet and the quintet respectively by $|s\rangle$ and $|1, 1; 2, S_z\rangle$. To investigate what kind of magnetic order is stabilized in the

condensate, let us introduce the following mean-field ansatz for the ground state:

$$|\{\theta_{\mathbf{r}}\}, \{\psi_{\mathbf{r}}\}\rangle = \bigotimes_{\mathbf{r} \in \text{plaq}} \left\{ \cos \theta_{\mathbf{r}} |s\rangle_{\mathbf{r}} + \sin \theta_{\mathbf{r}} \sum_{S_z=-2}^2 \psi_{\mathbf{r}}(S_z) |1, 1; 2, S_z\rangle_{\mathbf{r}} \right\}, \quad (31)$$

where the product is over all plaquettes and the complex numbers $\psi_{\mathbf{r}}(S_z)$ satisfy $\sum_{S_z} |\psi_{\mathbf{r}}(S_z)|^2 = 1$. Then, since the rank-1 tensor can not give rise to transitions between the spin-0 states and the spin-2 ones by the Wigner-Eckart theorem²⁷, we have $\langle s | S_i^\alpha | s \rangle = \langle s | Q_{ij}^{\alpha\beta} | s \rangle = 0$, $\langle s | S_i^\alpha | 1, 1; 2, S_z \rangle = 0$ and consequently $\langle \{\theta_{\mathbf{r}}\}, \{\psi_{\mathbf{r}}\} | \mathbf{S}_i | \{\theta_{\mathbf{r}}\}, \{\psi_{\mathbf{r}}\} \rangle = \mathbf{0}$. If we introduce the cyclic operator C which translates the state as $1 \rightarrow 2 \rightarrow 3 \rightarrow 4 \rightarrow 1$, we obtain $C|s\rangle = -|s\rangle$, $C|1, 1; 2, S_z\rangle = |1, 1; 2, S_z\rangle$ from (4) and (7). Therefore, the spin-nematic tensor $Q_{ij}^{\alpha\beta}$ defined on the bond (i, j) satisfies $\langle s | Q_{12}^{\alpha\beta} | 1, 1; 2, S_z \rangle = \langle s | C^\dagger C Q_{12}^{\alpha\beta} C^\dagger C | 1, 1; 2, S_z \rangle = -\langle s | Q_{23}^{\alpha\beta} | 1, 1; 2, S_z \rangle = \langle s | Q_{34}^{\alpha\beta} | 1, 1; 2, S_z \rangle = -\langle s | Q_{41}^{\alpha\beta} | 1, 1; 2, S_z \rangle$. This implies that the spinor condensate $|\{\theta_{\mathbf{r}}\}, \{\psi_{\mathbf{r}}\}\rangle$ of our quintet boson has the same (d -wave) symmetry as the spin-nematic state discussed in Ref.10.

However, this is not the end of the story. Since the local spin operator with $S \geq 1$ assumes several different states (e.g. *polarized*, *nematic*, etc.) and it is not obvious if $\langle \{\theta_{\mathbf{r}}\}, \{\psi_{\mathbf{r}}\} | Q_{ij}^{\alpha\beta} | \{\theta_{\mathbf{r}}\}, \{\psi_{\mathbf{r}}\} \rangle \neq 0$ or not for our J_1 - J_2 model. To determine the actual value of $\langle \{\theta_{\mathbf{r}}\}, \{\psi_{\mathbf{r}}\} | Q_{ij}^{\alpha\beta} | \{\theta_{\mathbf{r}}\}, \{\psi_{\mathbf{r}}\} \rangle$, we need the explicit mean-field solution for a given set of (J_1, J_2, λ) . Since we are considering the situation where the gap between the singlet ground state and the quintet excitation is vanishingly small, it would be legitimate to keep only the singlet $|0, 0, 0\rangle$ and the quintet for each plaquette to write down the effective Hamiltonian.

The form of the effective Hamiltonian is determined by using the second-order perturbation theory and it contains the kinetic part describing the hopping of the quintet particles and the magnetic part which concerns the interactions among them. Since within a mean-field treatment the spinor part $\psi_{\mathbf{r}}(S_z)$ is determined by the magnetic interactions, it suffices to consider only the magnetic part of the effective Hamiltonian:

$$H_{\text{qu}} = \sum_{\langle i, j \rangle} \left\{ J_{\text{qu}1} (\tilde{\mathbf{S}}_i^q \cdot \tilde{\mathbf{S}}_j^q) + K_{\text{qu}1} (\tilde{\mathbf{S}}_i^q \cdot \tilde{\mathbf{S}}_j^q)^2 \right\} + \sum_{\langle i', j' \rangle} \left\{ J_{\text{qu}2} (\tilde{\mathbf{S}}_{i'}^q \cdot \tilde{\mathbf{S}}_{j'}^q) + K_{\text{qu}2} (\tilde{\mathbf{S}}_{i'}^q \cdot \tilde{\mathbf{S}}_{j'}^q)^2 \right\} + \sum_{\langle i'', j'', k'' \rangle} \left\{ L_{\text{qu}1} \left\{ (\tilde{\mathbf{S}}_{i''}^q \cdot \tilde{\mathbf{S}}_{j''}^q) (\tilde{\mathbf{S}}_{i''}^q \cdot \tilde{\mathbf{S}}_{k''}^q) + (\tilde{\mathbf{S}}_{i''}^q \cdot \tilde{\mathbf{S}}_{k''}^q) (\tilde{\mathbf{S}}_{i''}^q \cdot \tilde{\mathbf{S}}_{j''}^q) \right\} + L_{\text{qu}2} \left\{ (\tilde{\mathbf{S}}_{i''}^q \times \tilde{\mathbf{S}}_{j''}^q) \cdot (\tilde{\mathbf{S}}_{i''}^q \times \tilde{\mathbf{S}}_{k''}^q) + (\tilde{\mathbf{S}}_{i''}^q \times \tilde{\mathbf{S}}_{k''}^q) \cdot (\tilde{\mathbf{S}}_{i''}^q \times \tilde{\mathbf{S}}_{j''}^q) \right\} \right\}, \quad (32)$$

where \tilde{S}^a denotes the $S = 2$ spin operator, and the symbols $\langle i, j \rangle$ and $\langle i', j' \rangle$ mean the nearest-neighbor- and the next-nearest-neighbor pairs, respectively. For different types of three-plaquette clusters $\langle i'', j'', k'' \rangle$, we assign different three-body (i.e. three-plaquette) interactions $L_{\text{qu}1,2}^{(n)}$ ($n = 1, \dots, 6$) in (32). The correspondence between six types of clusters and the strength of the three-plaquette interaction $L_{\text{qu}1,2}^{(n)}$ is shown in FIG. 11. The full expressions of $J_{\text{qu}1,2}$, $K_{\text{qu}1,2}$ and $L_{\text{qu}1,2}^{(n)}$ are given in Appendix. D. Note that our effective Hamiltonian in its full form contains the kinetic term and charge interactions as well as magnetic ones H_{qu} . In this sense, our effective model is a generalization of the Bose Hubbard Hamiltonian for $F = 2$ cold atoms in optical lattices^{29,30,31} and the determination of the full phase diagram and the identification of various phases found in systems of cold atoms in our magnetic system would be interesting in its own right.

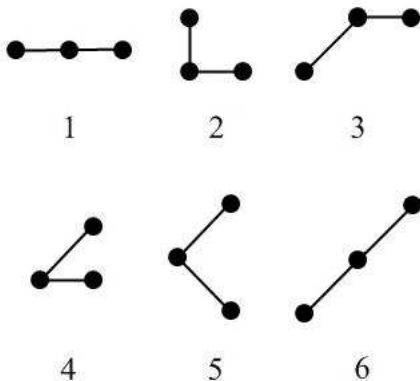


FIG. 11: Clusters involved in the 3-points interaction in (32). The plaquette corresponding to i'' is always located on the center of the clusters. We identify all clusters obtained from a given one by rotation by $\pi/2$, π , $3\pi/2$ and reflection.

We investigate this Hamiltonian by means of a mean-field theory by assuming an \mathbf{r} -independent uniform $\{\theta, \psi\}$, for simplicity. Since the parametrization of the spin-2 states is cumbersome, we adopt the method used by Bacry²⁸ and Barnett *et al.*²⁹. First we note that arbitrary (normalized) spin- S states are parametrized by a set of $2S$ unit vectors except for obvious gauge redundancy. Using rotational symmetry, we can further reduce the number of free parameters needed to express arbitrary spin-2 states to $2 \times 4 - 3 = 5$ (see Appendix. B). We numerically minimized the mean-field energy with respect to these five parameters. The result is shown in FIG. 12.

At $\lambda = 1$, the system is in the ferromagnetic state for $J_1/J_2 < -2.33$ and is in the spin-nematic state for $-2.33 \leq J_1/J_2 (\leq -1.91)$. This result slightly differs from the numerical results^{9,10} $-2.5 \lesssim J_1/J_2 \lesssim -1.43 \sim -1.67$. However, this is not surprising since our results are based on a mean-field treatment of the magnetic Hamiltonian H_{qu} obtained by perturbation expansion in λ . Our result may be improved by taking the number of sublattice larger, since $J_{\text{qu}2} > 0$ and there are various 3-site interactions $L_{\text{qu}1}$ and $L_{\text{qu}2}$.

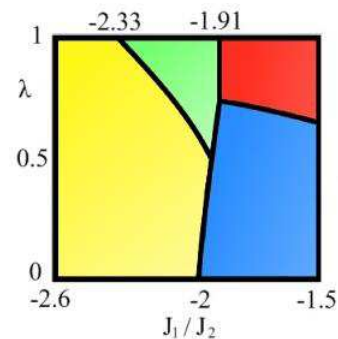


FIG. 12: The schematic phase diagram obtained in a similar manner to in FIG. 10. We zoom up the region around $J_1/J_2 = -2$ in FIG. 10. In the two regions on the left (green and yellow), the quintet and the singlet condense and we determined the resulting magnetic orders by a mean-field approximation to the magnetic Hamiltonian H_{qu} . In the green region, the quintet and the singlet condense, and the spin-nematic phase appears. In the red, on the other hand, conventional ferromagnetic order is stabilized. The red and the blue region are the same as FIG. 10.

V. MAGNETIZATION PROCESS

Having mapped out the phase diagram in the absence of external magnetic field, we consider next the magnetization process of the plaquette model by mapping the original model onto a hardcore boson model or an equivalent $S = 1/2$ pseudo-spin model. Tachiki and Yamada³² applied this method to obtain the magnetization curve of the spin-dimer model, which consists of pairs of $S = 1/2$ spins. The coupling to the external magnetic field is incorporated into the Hamiltonian by adding the Zeeman term $g\mu_B \mathbf{h} \cdot \sum_i \mathbf{S}_i$. For convenience, we set $g\mu_B = 1$ and assume that \mathbf{h} is pointing the z -direction: $\mathbf{h} = (0, 0, h)$.

Although the original treatment in Ref. 32 is for a coupled dimer systems, we can readily generalize the method to our plaquette system as follows. We denote the plaquette states by $|S_a, S_b; S, S^z\rangle$, where S, S_a, S_b are defined in (2). From (3), the energies of a single plaquette satisfy

$$E(1, 1, 2) < 2E(1, 0, 1), 2E(0, 1, 1), \quad (33)$$

for $-2 < J_1/J_2 < 0$. As is shown in FIG. 13, with increasing the magnetic field, the quintet level $|1, 1; 2, -2\rangle$ comes down to $|0, 0; 0\rangle$ faster than the lowest triplet levels $|1, 0; 1 - 1\rangle$ and $|0, 1; 1, -1\rangle$.

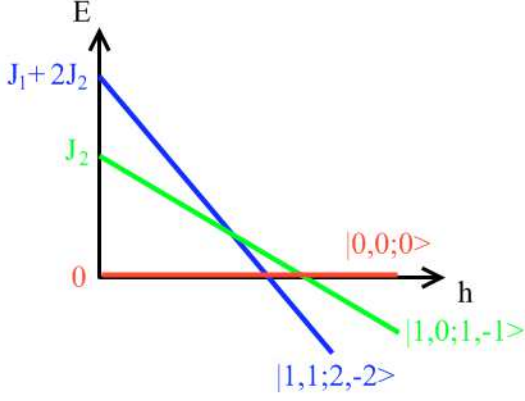


FIG. 13: The energy of eigenstates of a single plaquette as a function of magnetic field h .

Therefore, in order to describe the low-energy physics in the presence of strong magnetic field ($h \sim J_1/2 + J_2$), we may keep only the two lowest-lying states $|0, 0; 0\rangle$ and $|1, 1; 2, -2\rangle$ for each plaquette and restrict ourselves to the subspace spanned by them. In what follows, we regard the singlet $|0, 0; 0\rangle$ and the quintet $|1, 1; 2, -2\rangle$ respectively as the up- and the down state of a pseudo spin-1/2. That is,

$$|0, 0; 0\rangle = \begin{pmatrix} 1 \\ 0 \end{pmatrix}, \quad |1, 1; 2, -2\rangle = \begin{pmatrix} 0 \\ 1 \end{pmatrix}. \quad (34)$$

Then, the resulting effective Hamiltonian is written in terms of the Pauli matrices ($S = 1/2$ spins) defined on each strongly-coupled plaquette.

Note that the approximation to treat only the subspace

spanned by $|0, 0; 0\rangle$ and $|1, 1; 2, -2\rangle$ probably breaks down for $h \approx 0$ where all the components ($S^z = -2, \dots, 2$) of the quintet come into play. Also the validity of the approximation may be questionable for sufficiently large λ where the singlet-triplet gap may be much smaller than the singlet-quintet gap, since the triplet states $|1, 0; 1\rangle$ and $|0, 1; 1\rangle$ are important there (see FIG. 10).

If we simply project the original $S = 1/2$ Hamiltonian to the restricted subspace as in (8), no spin-flipping term (or, hopping term, in terms of hardcore bosons) appears. This is because the projection is equivalent to the ordinary first-order perturbation theory and no transition between the singlet and the quintet occurs in the first-order processes. Therefore, we need take into account the second-order processes to obtain the meaningful effective Hamiltonian. The amplitude that a quintet state (spin ‘down’) $|1, 1; 2, -2\rangle$ hops to the adjacent plaquette is given by

$$t \equiv \lambda^2 \frac{J_1^2 + J_2^2}{8J_1}. \quad (35)$$

The hopping to the next nearest-neighbor does not occur at this order of approximation. The energy gap between the state where there exists only one static ‘down’ spin ($|1, 1; 2, -2\rangle$) in a background of the ‘up’ spins (singlet $|0, 0; 0\rangle$ plaquettes) and the one where all plaquettes are ‘up’ is given by $-\mu$ in (D13a). The interaction between the two adjacent ‘up’ spins ($|1, 1; 2, -2\rangle$) is given by $J_{\text{eff}1}$ in (D13b) and that between the next-nearest-neighbor pair is given by $J_{\text{eff}2}$ in (D13c). We note that this approximation becomes poor near the pole of $J_{\text{eff}1,2}$ and t at $J_1/J_2 = 0$. On top of them, we have several three-‘site’ processes and putting them all together, we obtain the effective Hamiltonian:

$$\begin{aligned} H_{\text{eff}} = & (J_1 + 2J_2 - \mu - 2h) \sum_i \sigma_i^- \sigma_i^+ + \sum_{\langle i,j \rangle} \{t(\sigma_i^+ \sigma_j^- + \sigma_i^- \sigma_j^+) + J_{\text{eff}1}(\sigma_i^- \sigma_i^+)(\sigma_j^- \sigma_j^+)\} \\ & + \sum_{\langle i',j' \rangle} J_{\text{eff}2}(\sigma_{i'}^- \sigma_{i'}^+)(\sigma_{j'}^- \sigma_{j'}^+) + \sum_{\langle i'',j'',k'' \rangle} L_{\text{eff}}(\sigma_{i''}^+ \sigma_{i''}^-)(\sigma_{j''}^- \sigma_{j''}^+)(\sigma_{k''}^- \sigma_{k''}^+), \end{aligned} \quad (36)$$

where σ_s denote the Pauli matrices and $\sigma^+ = \frac{1}{2}(\sigma^x + i\sigma^y)$, $\sigma^- = \frac{1}{2}(\sigma^x - i\sigma^y)$. The symbols $\langle i, j \rangle$ and $\langle i', j' \rangle$ mean that the summation is taken over the nearest-neighbor and the next-nearest-neighbor plaquettes, respectively. As in section IV, there are six types of L_{eff} for different bond configurations $\langle i'', j'', k'' \rangle$ (see FIG. 11). We label the different three-plaquette interactions by $L_{\text{eff}}^{(n)}$ ($n = 1 \dots 6$) and the corresponding bond-configurations are shown in FIG. 11. The concrete expressions of J_{eff} and L_{eff} are given in Appendix. D. We note that the transverse components σ^+ and σ^- can be translated to the creation- a and the annihilation a^\dagger operator of a hardcore boson, respectively.

We analyze the Hamiltonian (36) within a mean-field approximation. Since $J_{\text{eff}1,2}$, which have the first order contributions in λ , are dominant for small λ , we may assume two different two-sublattice structures: (i) ‘‘checkerboard’’ and (ii) ‘‘stripe’’ shown in FIG. 14 in the calculation.

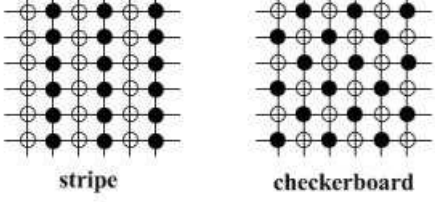


FIG. 14: Two-sublattice structures assumed in the calculation: (i) striped- (left) and (ii) checkerboard (right) case. Circles (whether filled or open) denote the strongly-coupled plaquettes shown by thick lines in FIG. 1.

By using the relations

$$\sigma^- \sigma^+ = \frac{1}{2}(1 - \sigma^z), \quad (37a)$$

$$\sigma_i^- \sigma_j^+ + \sigma_i^+ \sigma_j^- = \frac{1}{2}(\sigma_i^x \sigma_j^x + \sigma_i^y \sigma_j^y), \quad (37b)$$

we can rewrite (36) in terms of $\sigma^i (i = x, y, z)$. Since we are interested in the ground state energy at $T = 0$, we can simply replace operators in (36) by their expectation values on each site, e.g. $\sum_{\langle i,j \rangle} \sigma_i^z \sigma_j^z \rightarrow \sum_{\langle i,j \rangle} \langle \sigma^z \rangle \langle \sigma^{z'} \rangle$ for the “checkerboard” case. For convenience, we introduce the following two-component vector:

$$\boldsymbol{\tau} \equiv \begin{pmatrix} \langle \sigma^x \rangle \\ \langle \sigma^y \rangle \end{pmatrix}. \quad (38)$$

Since there is rotational symmetry in the x - y plane, the mean-field energy is parametrized by $\langle \sigma^z \rangle$, $\langle \sigma^{z'} \rangle$, $\tau \equiv |\boldsymbol{\tau}|$, $\tau' \equiv |\boldsymbol{\tau}'|$ and the angle ϕ between $\boldsymbol{\tau}$ and $\boldsymbol{\tau}'$. The Hamiltonian (36) reduces to

$$E_{\text{eff}} = N_p \left[\left(-\frac{(J_1 + 2J_2 - \mu - 2h)}{2} - \xi \right) \frac{(\langle \sigma^z \rangle + \langle \sigma^{z'} \rangle)}{2} + \alpha_1 \langle \sigma^z \rangle \langle \sigma^{z'} \rangle + \alpha_2 \frac{(\langle \sigma^z \rangle^2 + \langle \sigma^{z'} \rangle^2)}{2} \right. \\ \left. + \left(\beta_1 \tau \tau' \cos \phi + \beta_2 \frac{(\tau^2 + \tau'^2)}{2} \right) + \gamma_1 \frac{(\langle \sigma^z \rangle \langle \sigma^{z'} \rangle^2 + \langle \sigma^z \rangle^2 \langle \sigma^{z'} \rangle)}{2} + \gamma_2 \frac{(\langle \sigma^z \rangle^3 + \langle \sigma^{z'} \rangle^3)}{2} \right] \quad (39)$$

where N_p denotes the total number of plaquettes and $\alpha, \beta, \gamma, \xi$ are given in Appendix D both for the case of “checkerboard” and for the “striped” case. Correspondingly, the total magnetization is given simply as

$$M = \frac{1}{2N_p} \sum_{i \in \text{plaq}} (1 - \sigma_i^z). \quad (40)$$

In both cases, $\beta_{1,2} < 0$ and E_{eff} is minimized for $\phi = 0$. Since any spin-1/2 states satisfy the following relation among the expectation values (see eq. (C5))

$$\langle \sigma^z \rangle^2 + \tau^2 = 1, \quad (41)$$

the transverse magnetization τ can be expressed in terms of the longitudinal one $\langle \sigma^z \rangle$. Hence, there remain two variational parameters $\langle \sigma^z \rangle$ and $\langle \sigma^{z'} \rangle$ in E_{eff} . From the definition (34), the expectation values $\langle \sigma^z \rangle = 1$ and $\langle \sigma^z \rangle = -1$ respectively correspond to the singlet state and the fully polarized (or, saturated) state.

The critical field $h = H_{c1}$ which marks the onset of magnetization is given by $(\partial E_{\text{eff}} / \partial \langle \sigma^z \rangle)_{\langle \sigma^z \rangle = 1} = 0$ after substituting $\langle \sigma^{z'} \rangle = \langle \sigma^z \rangle$, i.e.

$$2H_{c1} = J_1 + 2J_2 - \mu + 4t. \quad (42)$$

The right-hand side is exactly the same as (27).

Once spin-gap closes at $h = H_{c1}$, the quintet particle $|1, 1; 2, -2\rangle$ condenses, i.e. $\langle \sigma^z \rangle \neq 1$, $\tau \neq 0$. If $\langle \sigma^z \rangle \neq \pm 1$, $\tau \neq 0$ and there exists a finite expectation value of $\langle \sigma^- \rangle$. In the hardcore boson language discussed below (36), σ^- can be viewed as the boson annihilation operator a and its finite expectation value $\langle a \rangle \neq 0$ implies that Bose-Einstein condensation of the quintet particle occurs. In particular, if $|\langle \sigma^z \rangle| \neq |\langle \sigma^{z'} \rangle|$ and $\tau \neq \tau'$ in BEC phase, the state is in the so-called “supersolid” phase³⁴. For convenience, we shall call the BEC phase satisfying $\langle \sigma^z \rangle = \langle \sigma^{z'} \rangle$ a *normal BEC*.

It should be noted that even when $\tau \neq 0$, the transverse magnetization $\langle S^\pm \rangle$ vanishes unlike the BEC in the spin-dimer model¹⁶. In fact, since the creation operator a^\dagger of the quintet particle can be written in terms of the original spin operators as

$$a^\dagger = \frac{1}{2} (Q_{B_1}^{xx} - Q_{B_1}^{yy}) + i Q_{B_1}^{xy} \\ = \frac{1}{2} (S_1^+ S_2^+ - S_2^+ S_3^+ + S_3^+ S_4^+ - S_4^+ S_1^+) \quad (43) \\ Q_{B_1}^{ab} \equiv Q_{12}^{ab} - Q_{23}^{ab} + Q_{34}^{ab} - Q_{41}^{ab},$$

the existence of the condensate $\langle \sigma^+ \rangle \neq 0$ (or $\tau \neq 0$) implies that we have a finite expectation value of the following spin-

nematic operator:

$$\left\langle \frac{1}{2} (Q_{B_1}^{xx} - Q_{B_1}^{yy}) \pm i Q_{B_1}^{xy} \right\rangle. \quad (44)$$

The form (43) of the quintet creation operator suggests that we should think of the plaquette quintet $|1, 1; 2, 2\rangle$ as a tightly-bound magnon pair (or *magnon molecule*).

The critical field H_{c2} where the saturation occurs is given by $(\partial E_{\text{eff}}/\partial \langle \sigma^z \rangle)_{\langle \sigma^z \rangle = -1} = 0$ after substituting $\langle \sigma^{z'} \rangle = \langle \sigma^z \rangle$, i.e.

$$2H_{c2} = J_1 + 2J_2 - \mu - 4t + 4J_{\text{eff}1} + 4J_{\text{eff}2} - 2L_{\text{eff}}^{(1)} - 8L_{\text{eff}}^{(3)} - 8L_{\text{eff}}^{(4)} - 2L_{\text{eff}}^{(6)}. \quad (45)$$

We minimized E_{eff} numerically and we found that the energy in the “stripe” case was always equal to or smaller than that in the “checkerboard” case. We show various types of magnetization curves obtained in this way in FIG. 16. In FIG. 15, we also classified the parameter regions (in the $(J_1/J_2, \lambda)$ -plane) according to the qualitative behavior of the magnetization curve. There appears (i) the normal BEC phase, (ii) the “striped” supersolid phase and (iii) the “striped” 1/2-plateau. At the 1/2-plateau, the pseudo-spins σ are ordered in a collinear manner $\langle \sigma^z \rangle = 1$ and $\langle \sigma^{z'} \rangle = -1$ (see FIG. 14).

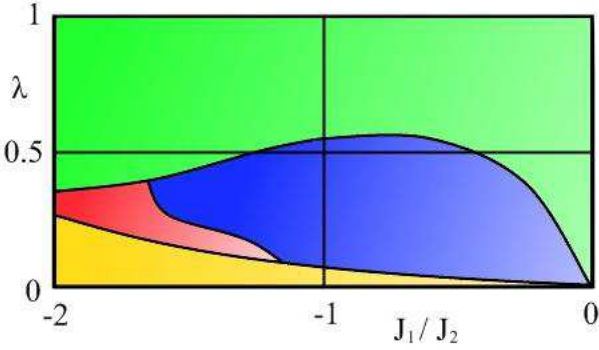


FIG. 15: Schematic classification of the magnetization curve. (i) In the green region, the curve is smooth and the system is always in the normal BEC phase. (ii) In the red region, the magnetization curve has a 1/2-plateau. Except at the plateau, the system is in the normal BEC phase. (iii) The region where we have additional supersolid phases around the 1/2-plateau is highlighted in blue. (iv) In the region colored by yellow magnetization jumps to saturation and the magnetization process is step-like. The concrete expression of curves is shown in FIG. 16. The phase boundary is only schematic.

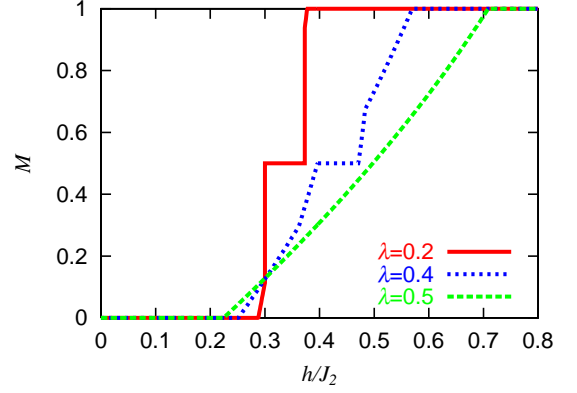


FIG. 16: Magnetization curve for various values of the distortion parameter λ . The frustration parameter is fixed to $J_1/J_2 = -1.4$. The colors of the curves correspond to those used in FIG. 15 (except for yellow). The blue curve has supersolid phase around the 1/2-plateau and the phase transition between the normal BEC and the supersolid phase is of second-order. All curves in BEC and supersolid phase is convex down because of the 3-point interaction γ in (39).

The magnetization curve in the BEC and the supersolid phase is convex down because of 3-point interaction γ in (39) which breaks the particle-hole symmetry. The “striped” supersolid phase always appears around the 1/2-plateau and the width of the supersolid phase appearing on the left of the 1/2 plateau is broader than that on the right due to the convex down character. The equivalent Hamiltonian (36) without the 3-point interactions has been investigated by using the mean field theory³⁵ and Monte-Carlo simulations^{35,36}. They found that the “striped” supersolid phase around the 1/2-plateau is stable³⁶. Therefore, our result that the supersolid phase exists may be correct beyond the mean-field approximation, since the 3-point interaction in (36) is weak. There are other models accompanied by the supersolid phase, e.g. spin dimer XXZ model³⁷, spin-1/2 XXZ model on the triangular lattice³⁸, etc.

VI. COMPARISON WITH THE EXPERIMENTAL DATA OF $(\text{CuCl})\text{LaNb}_2\text{O}_7$

In this section, we compare our results with the experimental data obtained for $(\text{CuCl})\text{LaNb}_2\text{O}_7$. Since we have three parameters J_1, J_2 and λ , three experimental inputs in principle determine the set of coupling constants. Then, we use those values of coupling constants to compare the magnetization curve of our model with the experimental one¹⁴.

We use the triplet gap $E_t^-(\mathbf{k} = \mathbf{0}) = 26.7\text{K}$ observed in inelastic neutron scattering¹³, the lower critical field $H_{c1} = 10.3\text{T}$ (or 15.0K if $g = 2.17$ is used), which marks the onset of magnetization, and the saturation field¹⁴ $H_{c2} = 30.1\text{T}$ (43.7K) as the experimental input.

The triplet gap has been calculated in sec. III and are given by eq.(D5) or (D6). In sec. V, we have obtained the critical field H_{c1} (eq.(42)) and H_{c2} (eq.(45)). We compare these results with the experimental ones to determine two exchange

couplings J_1 , J_2 and the distortion parameter λ . The result is:

$$J_1 = -140\text{K}, \quad J_2 = 87\text{K}, \quad \lambda = 0.46, \quad (46)$$

where we have used (D6) for the excitation energy of the triplet. The magnetization curve for the ratio $J_1/J_2 = -1.6$ and the distortion $\lambda = 0.46$ obtained above is shown in FIG. 17 (see FIG. 15). This curve is similar to that obtained in the high-field magnetization measurement¹⁴ except for the little convex down character.

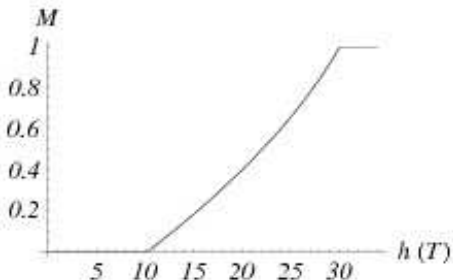


FIG. 17: Magnetization curve obtained from (39) by using the parameter set (46).

However, a remark is in order here. Recent NMR experiments²⁰ suggest the displacement patterns of Cl^- which yield different magnetic interactions from what have been assumed here. In particular, the system does not have any explicitly tetramerized structure (see FIG.1), although $(\text{CuCl})\text{LaNb}_2\text{O}_7$ has period 2 both in the a - and the b direction. Therefore, our results should not be taken literally. Instead, our plaquette model should be thought of as one of the simplest Hamiltonians realizing the BEC of magnon bound states which is applicable to much wider class of systems including our simple J_1 - J_2 model.

VII. CONCLUSION

Motivated by the recent discovery of a new two-dimensional spin-gap compound $(\text{CuCl})\text{LaNb}_2\text{O}_7$, we have studied spin-1/2 J_1 - J_2 model with a plaquette structure. For the small inter-plaquette interactions, i.e., for small λ , there exists a finite spin gap over the spin-singlet ground state.

We have computed the excitation energy of the triplets and the quintet in section III in two different methods. If the gap of the lowest excitation closes, the corresponding particle condenses and a phase transition occurs from a paramagnetic phase to magnetically ordered phases. For the case of ferromagnetic J_1 considered here, we have two possibilities. For relatively small $|J_1|/J_2$, the triplet particles (\mathbf{p} and \mathbf{q}) condense and generically we may expect CAF appears after the condensation (see FIG. 10).

For larger values of $|J_1|/J_2$, however, the quintet excitation matters and we may have various phases. In the situation of relevance, we have either a usual ferromagnetic phase or a less conventional spin-nematic phase. One of these phases

is selected by magnetic interaction among the quintet particles. We have derived an effective Hamiltonian governing the magnetic part by using the second-order perturbation and mapped out the magnetic phase diagram (see FIG. 12). A mean-field calculation predicted a finite window of the spin-nematic phase (green region in FIG. 12) in agreement with recent numerical results¹⁰ obtained for $\lambda = 1$. From the properties of the condensing particle, we found the nematic order for $-2.33 \leq J_1/J_2 \leq -1.91$ in the homogeneous ($\lambda = 1$) J_1 - J_2 model in section IV. We remark that our effective Hamiltonian is closely related to that for $F = 2$ cold atoms in optical lattices^{29,30,31}.

We have studied the magnetization process in section V. In the region of interest, magnetization is carried by spin-2 particles, which should be identified with a tightly-bound magnon pair (*magnon molecule*), and we have constructed an effective hardcore boson (or, pseudo spin-1/2) model for these spin-2 particles. By using a mean-field ansatz, we have determined the ground state of the above effective Hamiltonian as a function of the external field h . We have found three different phases: (i) the normal BEC phase, (ii) the ‘striped’ supersolid phase and (iii) the ‘striped’ 1/2-plateau. In the normal BEC phase, the transverse magnetization $\langle S^\pm \rangle$ vanishes unlike the conventional BEC in the spin-dimer model¹⁶.

We have compared the results obtained for our J_1 - J_2 model with the experimental data of $(\text{CuCl})\text{LaNb}_2\text{O}_7$ in section VI. Although we have found that our model could qualitatively explain the magnon gap in the inelastic neutron scattering experiments¹³ and the magnetization curve¹⁴, the structure suggested by NMR measurements²⁰ is inconsistent with our tetramerized J_1 - J_2 model and this agreement should not be taken literally. Nevertheless, we hope that our scenario ‘molecular spin-BEC’ based on a simple J_1 - J_2 model will capture the basic physics which underlies the magnetism of the compound $(\text{CuCl})\text{LaNb}_2\text{O}_7$.

ACKNOWLEDGMENTS

We would like to thank H. Kageyama for sharing his unpublished results, many helpful discussions, and comments on the manuscript. We are also grateful to A. Kitada and T. Miki for many useful discussions, and Mike Zhitomirsky for careful reading of the manuscript. This work is supported by the Grant-in-Aid for the 21st Century COE of Education, Culture, Sports, Science and Technology (MEXT) of Japan.

APPENDIX A: DIAGONALIZATION OF HAMILTONIAN BY BOGOLIUBOV TRANSFORMATION

For convenience, we briefly summarize the method of Bogoliubov transformation. We want to diagonalize

$$H = \sum_{\mathbf{k}} \mathbf{v}_{\mathbf{k}}^\dagger A(\mathbf{k}) \mathbf{v}_{\mathbf{k}}, \quad (\text{A1})$$

where

$$\mathbf{v}_{\mathbf{k}} = \left(p_{\mathbf{k}}, q_{\mathbf{k}}, p_{-\mathbf{k}}^{\dagger}, q_{-\mathbf{k}}^{\dagger} \right)^{\text{T}}, \quad (\text{A2a})$$

$$A(\mathbf{k}) = \begin{pmatrix} a(\mathbf{k}) & b(\mathbf{k}) & c(\mathbf{k}) & d(\mathbf{k}) \\ b(\mathbf{k}) & e(\mathbf{k}) & b(\mathbf{k}) & d(\mathbf{k}) \\ c(\mathbf{k}) & b(\mathbf{k}) & a(\mathbf{k}) & b(\mathbf{k}) \\ b(\mathbf{k}) & d(\mathbf{k}) & b(\mathbf{k}) & e(\mathbf{k}) \end{pmatrix}. \quad (\text{A2b})$$

Now p, q are boson operators, and $A(\mathbf{k}) = A(-\mathbf{k})$. We introduce Bogoliubov transformation

$$L_{\mathbf{k}} \mathbf{v}_{\mathbf{k}} = \mathbf{v}'_{\mathbf{k}}, \quad \mathbf{v}'_{\mathbf{k}} = \left(p'_{\mathbf{k}}, q'_{\mathbf{k}}, p_{-\mathbf{k}}^{\dagger}, q_{-\mathbf{k}}^{\dagger} \right)^{\text{T}}, \quad (\text{A3})$$

where L is 4×4 real matrix, and

$$\begin{aligned} L_{11}^*(\mathbf{k}) &= L_{33}(-\mathbf{k}), \quad L_{12}^*(\mathbf{k}) = L_{34}(-\mathbf{k}), \\ L_{13}^*(\mathbf{k}) &= L_{31}(-\mathbf{k}), \quad L_{14}^*(\mathbf{k}) = L_{32}(-\mathbf{k}), \\ &\vdots \end{aligned} \quad (\text{A4})$$

$$\begin{aligned} [p', p'^{\dagger}] &= [L_{1\mu} v_{\mu}, L_{1\nu} v_{\nu}^{\dagger}] = L_{11}^2 + L_{12}^2 - L_{13}^2 - L_{14}^2 = 1, \\ [p', q'^{\dagger}] &= L_{11}L_{21} + L_{12}L_{22} - L_{13}L_{23} - L_{14}L_{24} = 0, \\ [p'^{\dagger}, p'] &= L_{31}^2 + L_{32}^2 - L_{33}^2 - L_{34}^2 = -1, \\ &\vdots \end{aligned} \quad (\text{A5})$$

where the summation over repeated indices is implied. By using

$$g = \begin{pmatrix} 1 & 0 & 0 & 0 \\ 0 & 1 & 0 & 0 \\ 0 & 0 & -1 & 0 \\ 0 & 0 & 0 & -1 \end{pmatrix}, \quad (\text{A6})$$

and

$$\epsilon_i = \begin{cases} \epsilon = 1 & \text{for } i = 1, 2 \\ \epsilon = -1 & \text{for } i = 3, 4 \end{cases}, \quad (\text{A7})$$

the condition (A5) can be rewritten as

$$\mathbf{l}_i \cdot \mathbf{l}_j = g_{\mu\nu} l_i^{\mu} l_j^{\nu} = \epsilon_i \delta_{ij}, \quad L = \begin{pmatrix} \mathbf{l}_1^{\text{T}} \\ \mathbf{l}_2^{\text{T}} \\ \mathbf{l}_3^{\text{T}} \\ \mathbf{l}_4^{\text{T}} \end{pmatrix}. \quad (\text{A8})$$

where \mathbf{l} is a 4-dimensional column vector and the summation over i is not taken in (A8). $g_{\mu\nu}$ can be considered as a metric. The condition (A4) can be rewritten as

$$\mathbf{l}_{(3,4)}(-\mathbf{k}) = \begin{pmatrix} \mathbf{r}_{(1,2)}^{d*}(\mathbf{k}) \\ \mathbf{r}_{(1,2)}^{u*}(\mathbf{k}) \end{pmatrix}, \quad (\text{A9})$$

where $\mathbf{l}_i = (\mathbf{r}_i^{u\text{T}}, \mathbf{r}_i^{d\text{T}})^{\text{T}}$ and \mathbf{r} is a 2-dimensional column vector. We denote A in (A2b) as $A_{\mu\nu}$ and $\tilde{A} \equiv gA$ as

$A_{\nu}^{\mu} = g^{\mu\rho} A_{\rho\nu}$. Then, with regard to eigenvectors satisfying $A_{\nu}^{\mu} u_a^{\nu} = a u_a^{\mu}$, $A_{\nu}^{\mu} u_b^{\nu} = b u_b^{\mu}$, we obtain

$$\begin{aligned} g_{\mu\nu} u_a^{\mu} u_b^{\nu} &= u_{a\mu} u_b^{\mu} = \frac{1}{a} u_{a\mu} A_{\nu}^{\mu} u_b^{\nu}, \\ &= \frac{1}{b} u_{a\mu} A_{\nu}^{\mu} u_b^{\nu}, \end{aligned} \quad (\text{A10})$$

since $A_{\mu\nu}$ is symmetric. Therefore, if $a \neq b$, $u_{a\mu} u_b^{\mu} = 0$, i.e. eigenvectors of a different eigenvalue are orthogonal each other. We define

$$L' = (\mathbf{l}'_1 \ \mathbf{l}'_2 \ \mathbf{l}'_3 \ \mathbf{l}'_4)^{\text{T}} \quad (\text{A11})$$

where $\mathbf{l}'_i (i = 1 \sim 4)$ are eigenvectors of A_{ν}^{μ} , and

$$\mathbf{l}'_{(1,2)}{}^2 = 1, \quad \mathbf{l}'_{(3,4)}{}^2 = -1. \quad (\text{A12})$$

Then, $L' g L'^{\text{T}} = g$. Therefore,

$$L'^{\text{T}} g L' g = I, \quad (\text{A13})$$

where I is identity matrix. Now we can write

$$A = \begin{pmatrix} A_1 & A_2 \\ A_2 & A_1 \end{pmatrix}, \quad (\text{A14})$$

where $A_{1,2}$ are 2×2 matrix, and $A(\mathbf{k}) = A(-\mathbf{k})$. Therefore, we can take $\mathbf{l}'_i (i = 1 \sim 4)$ satisfying (A9). Defining Ω_i as the eigenvalue of $\mathbf{l}'_i (i = 1 \sim 4)$, this leads to

$$\Omega_1 = -\Omega_3, \quad \Omega_2 = -\Omega_4 \quad (\text{A15})$$

From (A13), (A1) reduces to

$$\begin{aligned} \mathbf{v}^{\dagger} A \mathbf{v} &= \mathbf{v}^{\dagger} g^2 A \mathbf{v} \\ &= \mathbf{v}'^{\dagger} L' g \tilde{A} L'^{\text{T}} \mathbf{v}' \\ &= \mathbf{v}'^{\dagger} L' g (\Omega_1 \mathbf{l}'_1 \ \Omega_2 \mathbf{l}'_2 \ \Omega_3 \mathbf{l}'_3 \ \Omega_4 \mathbf{l}'_4) \mathbf{v}' \\ &= \mathbf{v}'^{\dagger} \begin{pmatrix} \Omega_1 & 0 & 0 & 0 \\ 0 & \Omega_2 & 0 & 0 \\ 0 & 0 & -\Omega_3 & 0 \\ 0 & 0 & 0 & -\Omega_4 \end{pmatrix} \mathbf{v}' \end{aligned} \quad (\text{A16})$$

where $\mathbf{v}' = g L' g \mathbf{v}$, $\tilde{A} = gA$, and \mathbf{k} is omitted. Comparing to (A3), we obtain

$$L = g L' g. \quad (\text{A17})$$

This L satisfies (A8) and (A9). The eigenvalues of \tilde{A} (see eq. (A2b)) are given by

$$\begin{aligned} \Omega_{(\pm, \pm)} &= \pm [a^2 - c^2 - d^2 + e^2 \pm \{(-a^2 + c^2 + d^2 - e^2)^2 \\ &\quad + 4(a-d)(c-e)(-4b^2 + ac + cd + ae + de)\}^{\frac{1}{2}}]^{\frac{1}{2}}. \end{aligned} \quad (\text{A18})$$

We note that

$\Omega_{1,2}$ are the eigenvalues of the eigenvectors whose norm is positive, $\Omega_{3,4}$ are the eigenvalues of the eigenvectors whose norm is negative,

and (A15) is satisfied. Moreover, using the boson's commutation relation, H reduces to

$$H = \sum_{\mathbf{k}} \{ \omega_1(\mathbf{k}) p_{\mathbf{k}}^{\dagger} p'_{\mathbf{k}} + \omega_2(\mathbf{k}) q_{\mathbf{k}}^{\dagger} q'_{\mathbf{k}} \} + E_G, \quad (\text{A19a})$$

$$E_G = \sum_{\mathbf{k}} \frac{ \{ \omega_1(\mathbf{k}) + \omega_2(\mathbf{k}) \} }{2}. \quad (\text{A19b})$$

where $\omega_{1,2} = 2\Omega_{1,2}$.

APPENDIX B: HOW TO PARAMETRIZE GENERAL SPIN-S STATES

In this section, we briefly summarize the method of parametrizing arbitrary spin-2 states used in a mean-field calculation of section IV. The method is based on a geometrical representation of the spin- S states used by Bacry²⁸ and Barnett *et al.*²⁹. Since our model has rotational symmetry, the mean-field energy has a trivial degeneracy with respect to the global rotation of the spin states. To mod out this degeneracy and find only essentially different solutions, this geometric method is quite efficient.

First we introduce the maximally polarized spin- S state (*spin coherent state*) $|\hat{\Omega}\rangle$ which is pointing the direction of

$$\hat{\Omega} = (\cos \phi \sin \theta, \sin \phi \sin \theta, \cos \theta),$$

i.e. $(\mathbf{S} \cdot \hat{\Omega})|\hat{\Omega}\rangle = S|\hat{\Omega}\rangle$. If we introduce the Schwinger boson operators \hat{a}_+ (\hat{a}_-) which destroys a spin parallel (antiparallel) to the z -direction, the operator which creates a spin parallel to the $\hat{\Omega}$ -direction is given by

$$\hat{v}^{\dagger} = u\hat{a}_+^{\dagger} + v\hat{a}_-^{\dagger}, \quad (\text{B1})$$

where

$$u = e^{-i\frac{\chi}{2}} e^{-i\frac{\phi}{2}} \cos \frac{\theta}{2}, \quad v = e^{-i\frac{\chi}{2}} e^{i\frac{\phi}{2}} \sin \frac{\theta}{2} \quad (\text{B2})$$

and χ is an arbitrary gauge function. By using \hat{v}^{\dagger} , the coherent state $|\hat{\Omega}\rangle$ can be written simply as

$$\begin{aligned} |\hat{\Omega}\rangle &= \frac{1}{\sqrt{(2S)!}} (\hat{v}^{\dagger})^{2S} |0\rangle \\ &= v^{2S} \sum_{p=0}^{2S} \sqrt{{}_{2S}C_p} \left(\frac{u}{v}\right)^p |S : Sz = p - S\rangle, \end{aligned} \quad (\text{B3})$$

where the combinatorial symbol ${}_{2S}C_p$ is defined by ${}_{2S}C_p \equiv (2S)! / ((2S-p)!p!)$.

Next, we introduce a complex number $\zeta = (u/v)^* = e^{i\phi} \cot \frac{\theta}{2}$ and the corresponding unnormalized ket $|\zeta\rangle$:

$$|\zeta\rangle \equiv \sum_{p=0}^{2S} \sqrt{{}_{2S}C_p} (\zeta^*)^p |S : p - S\rangle. \quad (\text{B4})$$

We note that the vector $\hat{\Omega}$ rotates on the unit sphere S^2 , when the $SU(2)$ rotation operator \hat{D} acts on $|\zeta\rangle$. We denote an arbitrary spin- S state by $|A\rangle = \sum_{p=0}^{2S} A_p |S : p - S\rangle$. Then,

it is convenient to introduce the following ‘wave function’ which is in a one-to-one (except for an unphysical overall phase factor) correspondence with $|A\rangle$ under the condition $\sum |A|^2 = 1$:

$$\begin{aligned} P_s(\zeta) &\equiv \langle \zeta | A \rangle \\ &= \sum_{p=0}^{2S} \sqrt{{}_{2S}C_p} A_p \zeta^p \\ &= A_{2S} \prod_{i=1}^{2S} (\zeta - \alpha_i), \end{aligned} \quad (\text{B5})$$

where α_i s are the $2S$ roots of $P_s(\zeta) = 0$ and are parametrized as $\alpha_i = e^{i\phi_i} \cot \frac{\theta_i}{2}$. If the degree deg of the above polynomial is smaller than $2S$, $(2S - \text{deg})$ roots of $P_s(\zeta)$ are at the infinity ($\theta_i = 0$ or the north pole). Since the stereographic projection uniquely maps a set of $2S$ complex roots $\{\alpha_i\}$ onto a set of $2S$ points on a two-dimensional sphere S^2 , we can parametrize arbitrary spin- S states by specifying $2S$ points on a sphere.

If $A_{2S} = 0$, the limit $A_{2S} \rightarrow 0$, $\alpha_j = O(1/A_{2S})$ for any j must be taken ($\theta_j \rightarrow 0$). In the case of spin-2, $A'_i = A_i/A_{2S}$ is given in terms of four complex numbers $\{\alpha_i\}$ by

$$\begin{aligned} A'_0 &= \alpha_1 \alpha_2 \alpha_3 \alpha_4, \\ A'_1 &= -\frac{\alpha_1 \alpha_2 \alpha_3 + \alpha_1 \alpha_2 \alpha_4 + \alpha_1 \alpha_3 \alpha_4 + \alpha_2 \alpha_3 \alpha_4}{2}, \\ A'_2 &= \frac{\alpha_1 \alpha_2 + \alpha_1 \alpha_3 + \alpha_1 \alpha_4 + \alpha_2 \alpha_3 + \alpha_2 \alpha_4 + \alpha_3 \alpha_4}{\sqrt{6}}, \\ A'_3 &= -\frac{\alpha_1 + \alpha_2 + \alpha_3 + \alpha_4}{2}, \\ A'_4 &= 1, \end{aligned} \quad (\text{B6})$$

and hence the coefficients $\{A_i\}$ read

$$A_i = \frac{e^{i\phi}}{\sqrt{\sum_{i'=0}^4 |A'_{i'}|^2}} A'_i \quad (i = 0, \dots, 4), \quad (\text{B7})$$

where ϕ is the phase of A_4 . Therefore, as has been described above, arbitrary spin-2 states are parametrized by a set of four unit vectors and an overall phase factor. The rotational symmetry enables us to further reduce the number of free parameters by fixing α_1 and α_2 as:

$$\alpha_1 = 1, \quad \alpha_2 = e^{i\phi_2}, \quad \alpha_3 = e^{i\phi_3} \cot \frac{\theta_3}{2}, \quad \alpha_4 = e^{i\phi_4} \cot \frac{\theta_4}{2}. \quad (\text{B8})$$

Equations (B6)-(B8) express arbitrary (except for global rotation) spin-2 states in terms of five free parameters.

APPENDIX C: RELATION AMONG THE EXPECTATION VALUES OF SPIN-S OPERATORS

There exists a simple relation among the expectation values of spin- S operators. By spin- S operators, here we mean all independent (traceless) polynomials made up of the usual

spin- S operators \mathbf{S} . The spin 1 case has been considered by Chen and Levy³⁹ in the context of spin-nematic order. An arbitrary spin- S ket is written as

$$\mathbf{z} = \begin{pmatrix} z_1 \\ z_2 \\ \vdots \\ z_{2S+1} \end{pmatrix}, \quad (\text{C1})$$

where $\sum_i^{2S+1} |z_i|^2 = 1$. It is convenient to consider the Lie group $SU(2S+1)$ which naturally acts on the above $(2S+1)$ -dimensional space. Let us denote the generators T^a ($a = 1, \dots, (2S+1)^2 - 1$) of $SU(2S+1)$ and normalize them as

$$\text{Tr}(T^a T^b) = \frac{1}{2} \delta^{ab}. \quad (\text{C2})$$

Then, they satisfy

$$\sum_a T_{ij}^a T_{kl}^a = \frac{1}{2} \left(\delta_{il} \delta_{jk} - \frac{1}{2S+1} \delta_{ij} \delta_{kl} \right) \quad (\text{C3})$$

$(i, j, k, l = 1, \dots, 2S+1).$

Using this relation, we obtain

$$\begin{aligned} \sum_a \langle T^a \rangle^2 &= (z_i^\dagger T_{ij}^a z_j)(z_k^\dagger T_{kl}^a z_l) \\ &= \frac{1}{2} \left\{ z_i^\dagger z_j z_j^\dagger z_i - \frac{1}{2S+1} (z_i^\dagger z_i)(z_k^\dagger z_k) \right\} \\ &= \frac{S}{2S+1}, \end{aligned} \quad (\text{C4})$$

where the summation over repeated indices is implied. In spin-1/2 ($SU(2)$) case, T^a can be written as $\frac{1}{2} \sigma^a$, where σ is Pauli matrix. Therefore, this relation can be written as

$$\sum_{i=x,y,z} \langle \sigma_i \rangle^2 = 1, \quad (\text{C5})$$

APPENDIX D: EXPRESSIONS OF OMITTED EQUATIONS

Section III B:

The elements of the second-order hopping matrix (eq. (24)) are given by:

$$a(\mathbf{k}) \equiv -\lambda \frac{J_2}{2} f_+(\mathbf{k}) - \lambda^2 \frac{J_2}{4} f_+(\mathbf{k}) + \lambda^2 \left\{ \frac{-4J_1^5 + 3J_1^4 J_2 + 24J_1^3 J_2^2 - 25J_1^2 J_2^3 + 28J_1 J_2^4 - 28J_2^5}{8J_2(J_1 - 2J_2)(J_1 - J_2)(J_1 + 2J_2)} - \frac{J_2}{4} \right\}, \quad (\text{D1})$$

$$b(\mathbf{k}) \equiv -\lambda \frac{J_2}{2} f_-(\mathbf{k}) - \lambda^2 \frac{J_2}{4} f_-(\mathbf{k}) + \lambda^2 \left\{ \frac{-4J_1^5 + 3J_1^4 J_2 + 24J_1^3 J_2^2 - 25J_1^2 J_2^3 + 28J_1 J_2^4 - 28J_2^5}{8J_2(J_1 - 2J_2)(J_1 - J_2)(J_1 + 2J_2)} - \frac{J_2}{4} \right\}. \quad (\text{D2})$$

$$f_{\pm}(\mathbf{k}) \equiv \cos k_x + \cos k_y + \cos(k_x \pm k_y). \quad (\text{D3})$$

The second-order energy shift for the singlet ground state is calculated as(see eq. (25)):

$$\Delta E_s \equiv -\frac{3\lambda^2 (2J_1^2 + 3J_2^2)}{8J_2}. \quad (\text{D4})$$

The excitation gap of triplets from the second-order perturbation is given by:

$$\Delta_t \equiv E_t^-(\mathbf{k} = \mathbf{0}) = J_2 - \lambda \frac{3}{2} J_2 + \lambda^2 \frac{2J_1^5 - 3J_2 J_1^4 + J_2^2 J_1^3 - 2J_2^3 J_1^2 + 24J_2^4 J_1 - 24J_2^5}{8J_2 (J_2 - J_1) (2J_2 - J_1) (J_1 + 2J_2)}. \quad (\text{D5})$$

The modified excitation gap of triplets which is free from the pole $J_1 = 2J_2$ is given by:

$$\Delta_{t,\text{mod}} \equiv E_{t,\text{mod}}^-(\mathbf{k} = \mathbf{0}) = J_2 - \lambda \frac{3}{2} J_2 + \lambda^2 \frac{25J_1^2 - 65J_2^2}{144J_2}. \quad (\text{D6})$$

The excitation energy of quintet from the second-order perturbation is given by:

$$E_q(\mathbf{k}) = J_1 + 2J_2 + \lambda^2 \left\{ \frac{-14J_1^3 + 4J_2 J_1^2 + 15J_2^2 J_1 - 6J_2^3}{8J_1 (2J_1 - J_2)} + \frac{(J_1^2 + J_2^2)}{4J_1} (\cos k_x + \cos k_y) \right\}. \quad (\text{D7})$$

Section IV:

The parameters of the effective Hamiltonian (32) where the quintet condenses are given by:

$$J_{\text{qu1}} = \frac{1}{8} \lambda (J_1 + J_2) - \frac{\lambda^2 (59J_1^4 + 78J_2 J_1^3 + 60J_2^2 J_1^2 + 26J_2^3 J_1 + J_2^4)}{576J_1 (3J_1^2 + 4J_2 J_1 + J_2^2)}. \quad (\text{D8})$$

$$J_{\text{qu}2} = \frac{\lambda J_2}{16} - \frac{\lambda^2 J_2^2 (133J_1^2 + 76J_2J_1 + 7J_2^2)}{2304J_1(3J_1^2 + 4J_2J_1 + J_2^2)}. \quad (\text{D9})$$

$$K_{\text{qu}1} = -\lambda^2 \frac{49J_1^4 + 174J_2J_1^3 + 120J_2^2J_1^2 + 10J_2^3J_1 - J_2^4}{2304J_1(3J_1^2 + 4J_2J_1 + J_2^2)}, \quad K_{\text{qu}2} = -\lambda^2 \frac{11J_2^4 + 68J_1J_2^3 + 137J_1^2J_2^2}{9216J_1(3J_1^2 + 4J_2J_1 + J_2^2)}. \quad (\text{D10})$$

$$\begin{aligned} L_{\text{qu}1}^{(1)} &= \frac{\lambda^2 (J_1 + J_2)}{576}, \quad L_{\text{qu}1}^{(2)} = 0, \quad L_{\text{qu}1}^{(3)} = \frac{\lambda^2 J_2}{1152}, \\ L_{\text{qu}1}^{(4)} &= -\frac{\lambda^2 J_2}{1152}, \quad L_{\text{qu}1}^{(5)} = \frac{\lambda^2 J_2^2}{4608J_1}, \quad L_{\text{qu}1}^{(6)} = -\frac{\lambda^2 J_2^2 (J_2 - 3J_1)}{4608J_1 (J_1 + J_2)}, \end{aligned} \quad (\text{D11})$$

$$L_{\text{qu}2}^{(i)} = -2L_{\text{qu}1}^{(i)}, \quad \text{for } i = 1, \dots, 6. \quad (\text{D12})$$

Section V:

The parameters of the effective Hamiltonian H_{eff} (36) in the magnetization process are given in a series in λ by:

$$-\mu \equiv \frac{\lambda^2 (-14J_1^3 + 4J_2J_1^2 + 15J_2^2J_1 - 6J_2^3)}{8J_1(2J_1 - J_2)}. \quad (\text{D13a})$$

$$J_{\text{eff}1} \equiv \lambda \frac{J_1 + J_2}{2} + \lambda^2 \frac{(6J_1^4 + 11J_2J_1^3 + 2J_2^2J_1^2 - 13J_2^3J_1 + 4J_2^4)}{16J_1(2J_1 - J_2)J_2}. \quad (\text{D13b})$$

$$J_{\text{eff}2} \equiv \lambda \frac{J_2}{4} + \lambda^2 \frac{J_2(6J_1^2 - 13J_2J_1 + 4J_2^2)}{32J_1(2J_1 - J_2)}. \quad (\text{D13c})$$

On top of them, we have three-body (or, three-plaquette) interactions:

$$L_{\text{eff}}^{(1)} = \lambda^2 \frac{(J_1 + J_2)^2}{4J_2}, \quad L_{\text{eff}}^{(2)} = 0, \quad L_{\text{eff}}^{(3)} = \frac{\lambda^2}{8} (J_1 + J_2), \quad L_{\text{eff}}^{(4)} = -\frac{\lambda^2}{8} (J_1 + J_2), \quad L_{\text{eff}}^{(5)} = 0, \quad L_{\text{eff}}^{(6)} = \lambda^2 \frac{J_2}{8}. \quad (\text{D13d})$$

The parameters necessary for the mean-field energy (39) in the external magnetic field depend on the sublattice structures assumed in the calculation and are given as follows.

1. In the case of “checkerboard” sublattice:

$$\begin{aligned} \xi &= J_{\text{eff}1} + J_{\text{eff}2} + \frac{1}{4}L_{\text{eff}}^{(1)} + L_{\text{eff}}^{(3)} + L_{\text{eff}}^{(4)} + \frac{1}{4}L_{\text{eff}}^{(6)}, \\ \alpha_1 &= \frac{1}{2} \left(J_{\text{eff}1} - L_{\text{eff}}^{(1)} \right), \quad \alpha_2 = \frac{1}{4} \left(2J_{\text{eff}2} + L_{\text{eff}}^{(1)} - 4L_{\text{eff}}^{(3)} - 4L_{\text{eff}}^{(4)} - L_{\text{eff}}^{(6)} \right), \\ \beta_1 &= t, \quad \beta_2 = 0, \quad \gamma_1 = \frac{1}{4}L_{\text{eff}}^{(1)} + L_{\text{eff}}^{(3)} + L_{\text{eff}}^{(4)}, \quad \gamma_2 = \frac{1}{4}L_{\text{eff}}^{(6)}. \end{aligned} \quad (\text{D14})$$

2. In the case of “striped” sublattice:

$$\begin{aligned} \xi &= J_{\text{eff}1} + J_{\text{eff}2} + \frac{1}{4}L_{\text{eff}}^{(1)} + L_{\text{eff}}^{(3)} + L_{\text{eff}}^{(4)} + \frac{1}{4}L_{\text{eff}}^{(6)}, \\ \alpha_1 &= \frac{1}{4} \left(J_{\text{eff}1} + 2J_{\text{eff}2} - L_{\text{eff}}^{(1)} - 4L_{\text{eff}}^{(3)} - 4L_{\text{eff}}^{(4)} - 2L_{\text{eff}}^{(6)} \right), \quad \alpha_2 = \frac{1}{4} \left(J_{\text{eff}1} + L_{\text{eff}}^{(6)} \right), \\ \beta_1 &= \frac{t}{2}, \quad \beta_2 = \frac{t}{2}, \quad \gamma_1 = \frac{1}{8} \left(L_{\text{eff}}^{(1)} + 8L_{\text{eff}}^{(3)} + 8L_{\text{eff}}^{(4)} + 2L_{\text{eff}}^{(6)} \right), \quad \gamma_2 = \frac{1}{8}L_{\text{eff}}^{(1)}. \end{aligned} \quad (\text{D15})$$

¹ H.T. Diep, *Frustrated Spin Systems*, edited by H.T. Diep (World Scientific, Singapore, 2004).

² P. Chandra and B. Doucot, Phys.Rev. B **38**, 9335 (1988).

³ H.J. Schulz, T.A.L. Ziman and D. Poilblanc, J.Phys. I **6** 675

- (1996).
- ⁴ L. Capriotti, F. Becca, A. Parola, and S. Sorella, *Phys.Rev.Lett.* **87**, 097201 (2001).
 - ⁵ R.R.P. Singh, Z. Weihong, C.J. Hamer, and J. Oitmaa, *Phys. Rev. B* **60**, 7278 (1999).
 - ⁶ V. Kotov, J. Oitmaa, O. Sushkov and Z. Weihong, *Phil. Mag. B* **80**, 1483 (2000).
 - ⁷ G. Misguich and C. Lhuillier, in Ref. 1.
 - ⁸ J. Oitmaa, C. Hamer and W. Zheng, *Series Expansion Methods for Strongly Interacting Lattice Models* (Cambridge University Press, UK, 2006).
 - ⁹ N. Shannon, B. Schmidt, K. Penc and P. Thalmeier, *Eur. Phys. J. B* **38**, 599 (2004).
 - ¹⁰ N. Shannon, T. Momoi and P. Sindzingre, *Phys. Rev. Lett.* **96**, 027213 (2006).
 - ¹¹ R. Melzi, P. Carretta, A. Lascialfari, M. Mambrini, M. Troyer, P. Millet, and F. Mila, *Phys. Rev. Lett.* **85**, 1318 (2000).
 - ¹² E.E. Kaul, H. Rosner, N. Shannon, R.V. Shapanchenko, and C. Geibel, *J. Mag. Mat.* **272-276**, 922 (2004).
 - ¹³ H. Kageyama, T. Kitano, N. Oba, M. Nishi, S. Nagai, K. Hirota, L. Viciu, J.B. Wiley, J. Yasuda, Y. Baba, Y. Ajiro and K. Yoshimura, *J. Phys. Soc. Jpn.* **74**, 1702 (2005).
 - ¹⁴ H. Kageyama, J. Yasuda, T. Kitano, K. Totsuka, Y. Narumi, M. Hagiwara, K. Kindo, Y. Baba, N. Oba, Y. Ajiro and K. Yoshimura, *J. Phys. Soc. Jpn.* **74**, 3155 (2005).
 - ¹⁵ T. Nikuni, M. Oshikawa, A. Oosawa and H. Tanaka, *Phys. Rev. Lett.* **84**, 5868 (2000).
 - ¹⁶ H. Tanaka, A. Oosawa, T. Kato, H. Uekusa, Y. Ohashi, K. Kakurai and A. Hoser, *J. Phys. Soc. Jpn.* **70**, 939 (2001).
 - ¹⁷ M. Jaime *et al.*, *Phys. Rev. Lett.* **93**, 087203 (2004); S.E. Sebastian *et al.*, *Phys. Rev. B* **72**, 100404 (2005).
 - ¹⁸ M.B. Stone, C. Broholm, D.H. Reich, O. Tchernyshyov, P. Vorderwisch and N. Harrison, *Phys. Rev. Lett.* **96**, 257203 (2006).
 - ¹⁹ A. Kitada, Z. Hiroi, Y. Tsujimoto, T. Kitano, H. Kageyama, Y. Ajiro and K. Yoshimura, *J. Phys. Soc. Jpn.* **76**, 093706 (2007).
 - ²⁰ M. Yoshida *et al.*, [arXiv:cond-mat/07063559]; submitted to *J. Phys. Soc. Jpn.*
 - ²¹ T. Momoi and K. Totsuka, *Phys. Rev. B* **62**, 15067 (2000).
 - ²² K. Totsuka, S. Miyahara and K. Ueda, *Phys.Rev.Lett.* **86**, 520 (2001).
 - ²³ S. Miyahara and K. Ueda, *J.Phys.: Condens. Matter* **15**, R327 (2003).
 - ²⁴ H. Nojiri, H. Kageyama, Y. Ueda and M. Motokawa, *J.Phys.Soc.Jpn.* **72**, 3243 (2003).
 - ²⁵ R. Bendjama, B. Kumar and F. Mila, *Phys. Rev. Lett.* **95**, 110406 (2005).
 - ²⁶ S. Sachdev and R. N. Bhatt, *Phys. Rev. B* **41**, 9323 (1990).
 - ²⁷ J.J. Sakurai, *Modern quantum Mechanics, ch.3* (Benjamin/Cummings Publishing Company, Inc. 1985).
 - ²⁸ H. Bacry, *J.Math.Phys.* **15**, 1686 (1974).
 - ²⁹ R. Barnett, A. Turner and E. Demler, *Phys.Rev.Lett.* **97**, 180412 (2006).
 - ³⁰ Fei Zhou and G.W. Semenov, *Phys.Rev.Lett.* **97**, 180411 (2006).
 - ³¹ M. Lewenstein, A. Sanpera, V. Ahufinger, B. Damski, A. Sen and U. Sen, *Adv.Phys.* **56**, 243 (2007).
 - ³² M. Tachiki and T. Yamada, *J. Phys. Soc. Jpn.* **28**, 1413 (1970).
 - ³³ M.E. Zhitomirsky and K. Ueda, *Phys. Rev. B* **54**, 9007 (1996).
 - ³⁴ A.F. Andreev and I.M. Lifshitz, *JETP*, **29** 1107, (1969); A.J. Leggett, *Phys. Rev. Lett.* **30**, 1543 (1970); K-S. Liu and M.E. Fisher, *J. Low. Temp. Phys.* **10**, 655 (1973).
 - ³⁵ R.T. Scalettar, G.G. Batrouni, A.P. Kampf and G.T. Zimanyi, *Phys. Rev. B*, **51**, 8467 (1995).
 - ³⁶ G.G. Batrouni and R.T. Scalettar, *Phys. Rev. Lett.* **84**, 1599 (2000); F. Hébert, G.G. Batrouni, R.T. Scalettar, G. Schmid, M. Troyer and A. Dorneich, *Phys. Rev. B*, **65**, 014513 (2001).
 - ³⁷ K.K. Ng and T.K. Lee, *Phys. Rev. Lett.* **97**, 127204 (2006); N. Laflorencie and F. Mila, *Phys. Rev. Lett.* **99**, 027202 (2007).
 - ³⁸ G. Murthy *et al.*, *Phys. Rev. B*, **55**, 3104 (1997); M. Boninsegni, *J. Low Temp. Phys.* **132**, 39 (2003); S. Wessel *et al.*, *Phys. Rev. Lett.* **95**, 127205 (2005); D. Heidarian *et al.*, *ibid* **95**, 127206 (2005); R. G. Melko *et al.*, *ibid* **95**, 127207 (2005); M. Boninsegni *et al.*, *ibid* **95**, 237204 (2005).
 - ³⁹ H.H. Chen and P.M. Levy, *Phys. Rev. B*, **7**, 4267 (1973).